Quaternary Science Reviews 101 (2014) 91–110

Contents lists available at ScienceDirect

Quaternary Science Reviews

journal homepage: www.elsevier.com/locate/quascirev

Late Pleistocene and Holocene palaeoenvironments in and around the middle Caspian basin as reconstructed from a deep-sea core

Suzanne A.G. Leroy [a, *], Lourdes López-Merino [a], Alina Tudryn [b, c], Françoise Chalié [d], Françoise Gasse [d, 1]

[a] Institute for the Environment, Brunel University, Uxbridge, UB8 3PH, London, UK
[b] Université Paris-Sud, Laboratoire GEOPS, UMR8148, Orsay, F-91405, France
[c] CNRS, Orsay, F-91405, France
[d] CEREGE, Aix-Marseille Université UM 34 – CNRS UMR 7330, Europôle Méditerranéen de l'Arbois, BP80, F-13545, Aix-en-Provence cedex 04, France

ARTICLE INFO

Article history:
Received 11 May 2014
Received in revised form
9 July 2014
Accepted 10 July 2014
Available online 26 July 2014

Keywords:
Caspian Sea
Pollen
Vegetation history
Dinocysts
Lake level fluctuation
Salinity
Late Pleistocene
Holocene

ABSTRACT

Late Pleistocene and/or Holocene high-resolution palynological studies are available for the south basin of the Caspian Sea (CS), the world's largest lake. However, the north and middle basins have not been the object of high-resolution palynological reconstructions. This new study presents the pollen, spores and dinoflagellate cysts records obtained from a 10 m-long sediment core recovered in the middle basin, which currently has brackish waters and is surrounded by arid and semi-arid vegetation.

An age–depth model built based on six radiocarbon dates on ostracod shells indicates that the sequence spans the period from 14.47 to 2.43 cal. ka BP. The present palaeoenvironmental study focuses on the top 666 cm, or from 12.44 to 2.43 cal. ka BP.

At the vegetation level, the Younger Dryas is characterised by an open landscape dominated by desert vegetation composed by Amaranthaceae with shrubs and salt-tolerant plants. However, although the Early Holocene is also characterised by desert vegetation, it is enriched in various shrubs such as *Ephedra* and *Calligonum*, but tree expansion is not important at the Holocene onset. After a major shift at 8.19 cal. ka BP, the Middle Holocene displays now both the character of desert and of steppe, although some trees such as *Quercus* and *Corylus* slightly spread. The Late Holocene records steppe vegetation as dominant, with more tree diversity.

Regarding the lacustrine signal, the dinocyst assemblage record fluctuates between slightly brackish conditions highlighted by *Pyxidinopsis psilata* and *Spiniferites cruciformis*, and more brackish ones – similar to the present day – with the dominance of *Impagidinium caspienense*. The Late Pleistocene is characterised by low salinities, related to the Khvalynian highstand. From 11.56 cal. ka BP, slightly more saline waters are reconstructed with an increase of *I. caspienense* for a period of 1000 years, which could be attributed to the Mangyshlak lowstand. From 10.55 cal. ka BP, low salinity conditions return with remains such as *Anabaena* and *Botryococcus* abundant until 8.83 cal. ka BP, followed by a slow, progressive decrease of *P. psilata* and *S. cruciformis* until 4.11 cal. ka BP, which is the main assemblage change at lacustrine scale. Since then, higher salinities, similar to the present one, are reconstructed. Finally, *Lingulodinium machaerophorum* starts its development only at 2.75 cal. ka BP, in the Late Holocene.

The present research revealed fundamental differences from previously published sea-level curves, in that a 6000 yr-long highstand suggested by low salinities is shown between 10.55 and 4.11 cal. ka BP. Amongst other arguments, using a comparison to a similar palynological regard but in the south basin, a N–S salinity gradient that is the reverse of the present one across the CS, suggests that the Amu Darya was flowing in the CS. Hence the CS levels during the Late Pleistocene and Holocene were influenced by a combination of precipitation over the high European latitudes and the indirect influence of the Indian summer monsoon over the Pamirs.

* Corresponding author.
E-mail address: suzanne.leroy@brunel.ac.uk (S.A.G. Leroy).
[1] Deceased at the end of manuscript preparation.

http://dx.doi.org/10.1016/j.quascirev.2014.07.011

1. Introduction

The Caspian Sea (CS) forms a natural geographical border between Europe and Asia at 50° east of longitude. It is the world's largest inland water body, with a current size equivalent to Norway (Fig. 1). Its level has changed dramatically over various timescales, causing rapid modifications in the volume and the area of the water body (Kazancı et al., 2004). During the 20th century, the CS water levels have fluctuated suddenly, a hundred times faster than recent global sea level rise (Kroonenberg et al., 2007). This caused serious environmental and economic damages and adversely affected oil and gas exploration and exploitation, agriculture and fishing (such as sturgeon for caviar). In addition, it caused major risks in areas used for storage of nuclear wastes and for nature conservation of international importance. Despite the importance of this area, no enough in-depth high-resolution palaeoenvironmental research has been performed on the CS sediments and the precise timing of these changes and even their causes remain not well understood yet. They have been suggested to be a combination of climate, human impact and tectonic activity (e.g. Shiklomanov et al., 1995; Froehlich et al., 1999), with a large role played by the precipitation over the Volga drainage basin (Arpe et al., 2012). However, the picture seems to be more complex, as not only the abovementioned factors affect the CS levels, but also the CS itself has an effect on the sub-tropical jet-stream speed via a lake effect on over-lake temperature, transferred to altitude. Hence its correct representation over time, especially its changing area during lowstands (such as the Mangyshlak lowstand at the beginning of the Holocene) and highstands (such at the Late Khvalynian highstand during the last period of melting of the Eurasian icesheet), in the general circulation models is essential (Farley Nicholls and Toumi, 2013).

The rare studies available so far on the palaeoenvironment of the CS during the Late Pleistocene and Holocene have been made on coastal sequences (e.g. Leroy et al., 2013a and references in it; Richards et al., in press) or in the shallow North basin (Bezrodnykh et al., 2004) and suffer from deposition hiatuses during periods of low sea levels and sedimentation starvation. Only one sequence provides continuous pollen and organic-walled dinoflagellate cysts (dinocyst) records of changes in the south basin from the Late Pleistocene to the Middle Holocene (Leroy et al., 2013c). Hardly anything is known for the middle basin, besides a preliminary pollen study by Kuprin and Rybakova (2003), but with a timescale based on a chronology built from bulk radiocarbon dates. No palynological studies (pollen and dinocysts) have been carried out on continuous, long sequences in the north basin.

The aim of this investigation is to partially fill this research gap by reconstructing changes in terrestrial vegetation and lake levels, mostly via salinity changes, that occurred in the middle basin of the

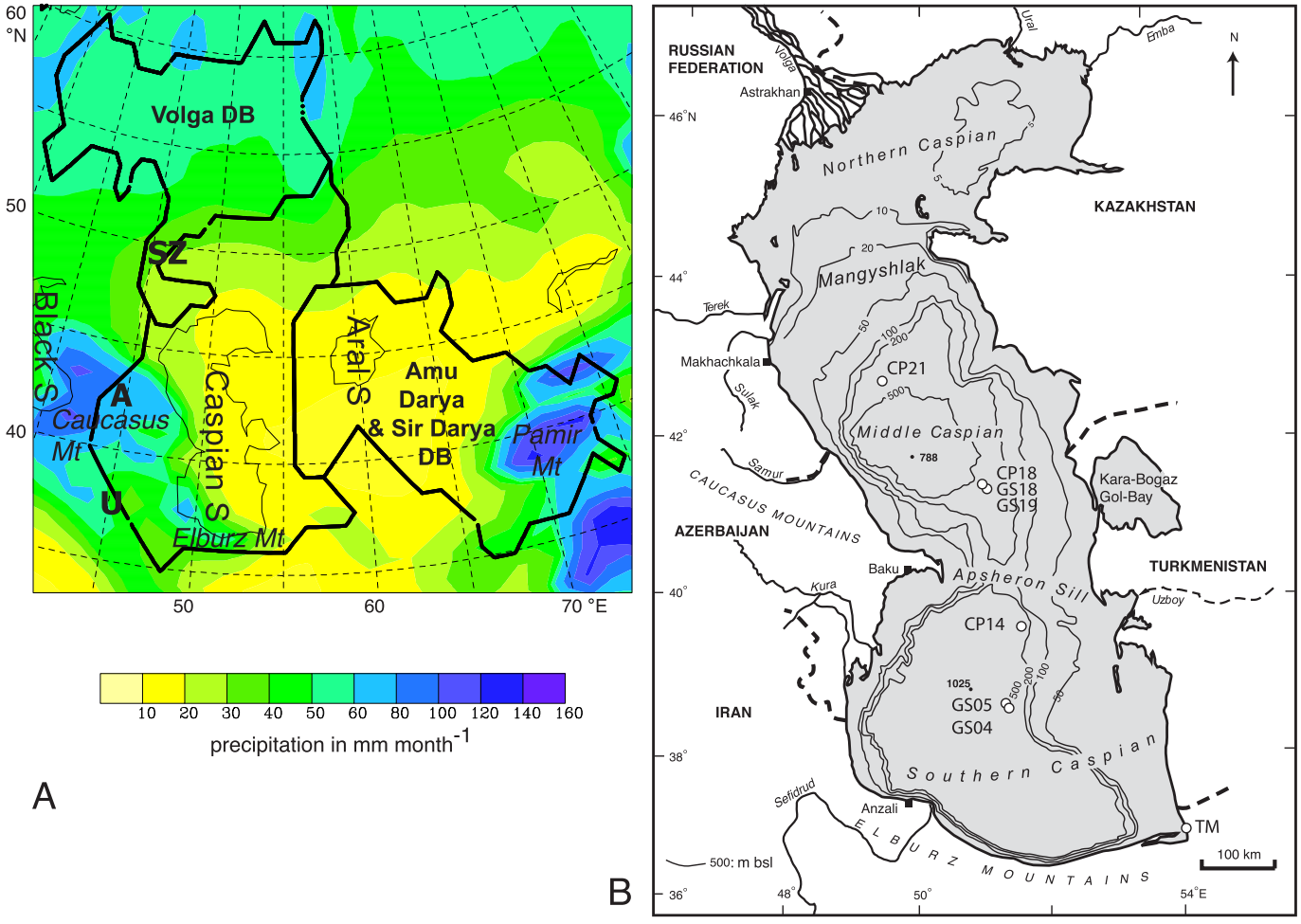

Fig. 1. Location map of the main inflows to the Caspian Sea (1A) and the cores (1B). For 1A: Black dashes lines are borders. Grey lines are rivers, continuous line for permanent, dashed line for temporary, SZ: Lake Solenoye Zaimishche, A: Lake Aligol, U: Lake Urmia, DB: drainage basin, S: Sea, Mt: Mountain. For 1B: Grey circles for core locations. Adapted from: Leroy et al. (2013c).

CS during the Late Pleistocene and the Holocene through palynological analyses. The chronology of the studied sequence is based on an age–depth model built from radiocarbon dating on ostracod shells. Additionally since similar analyses exist for the south basin, a comparison between the two main CS basins becomes possible and has the potential to highlight spatial gradients.

2. Study area

The physical and biological characteristics of the CS (36–47°N, 47–54°E, altitude of 26.5 m below sea level) have been summarised in some recent compilations such as by Kosarev and Yablonskaya (1994) and Kostianoy and Kosarev (2005), as well as in several recent papers (Leroy et al., 2013a,b). The CS is a large endorheic water body made up of three basins, deepening from the very shallow north (5–10 m deep) to the deepest south (maximal water depth 1025 m). The middle basin (138,000 km^2) has an average depth of 175 m and a maximum depth of 788 m (Fig. 1B).

2.1. Relief and vegetation

The middle basin is separated from the northern very shallow basin by the Mangyshlak Threshold, i.e. a sharp southwards drop of the bathymetry (Putans et al., 2010) (Fig. 1B). The east–west Apsheron Sill separates the south basin from the middle one with very shallow water depths of c. 80 m. The sill is the submarine link between the Great Caucasus and the Great Balkhan Mountains and a region of very active tectonics (Jackson et al., 2002). A North–South sharp trench in its middle down to c. 180 m bsl is the trace of an ancient river (Ferronsky et al., 1999). When the levels of the CS are low this threshold enforces a deep division in the two separate water bodies.

Specifically for the middle basin, the relief on the west coast goes from the high altitudes of the eastern end of the Great Caucasus Mountains to areas below sea levels. The rest of the coast is formed by lowlands that were flooded during the past periods of high CS levels (Kroonenberg et al., 2007). Overall the climate around the middle basin is under the influence of the westerlies, although it has its own local low-level circulation which is more N–S oriented (Leroy et al., 2011).

Vegetation west and east of the middle basin has a Kazakho-Dsungarian character with summer rainfall in the north, which acquires an Irano-Turanian character south-eastward with winter rainfall (Walter and Breckle, 1989). Along the west coast of the middle basin, the vegetation in Dagestan changes rapidly from a coastal semi-arid vegetation to the forests of the Caucasus with summer rainfall. An altitudinal forest zonation is visible, from the bottom up: *Quercus*, *Fagus*, *Abies*, *Picea*, *Betula* and finally *Pinus*. The capital city of Azerbaijan, Baku, situated on the coast, has a desert climate (Walter and Breckle, 1989). Along the coast of Turkmenistan, a semi-desert with halophytes, shrubs and semi-shrubs and herbaceous plants or a desert occurs. Freshwater holes arise in the desert between the Aral Sea and the CS, which are characterised by a local vegetation made of *Populus*, *Elaeagnus*, *Salix* and *Alnus*, as well as *Calligonum* and *Tamarix*.

2.2. Hydrological setting and sea level history

In general, water inputs to the CS comprise river discharges in particular the Volga (contributing up to 80–85% of the total) (Rodionov, 1994). Additionally, a series of very small rivers bring water from the west (e.g. Samur, Terek and Sulak Rivers to the middle basin) and south side of the CS (i.e. the Sefidrud and the Kura river), while the east side of the CS has hardly any rivers owing to a the dry climate (Lahijani et al., 2008). However, the largest amount of sediment is brought by smaller rivers, such as the Sefidrud and the Kura, in the south basin. This asymmetric pattern of river inflow induces a North–South positive gradient of water **salinity**, close to zero in the north and 14 psu in the south. The salinity of the middle basin is around 12–13 psu, becoming slightly higher along the eastern coast: 13–14 psu, fairly similar to that of the south basin (Tuzhilkin et al., 2005).

Surface water **temperatures** present important seasonal variations from the north to the south of the middle basin. The Northern basin surface water freezes from December to March, but this hardly reaches the middle basin (Kosarev, 2005). The mean water temperature reaches 24 °C during the warmest summer months, i.e. July and August, but falls to 7 °C in winter (Ginzburg et al., 2005).

The **current** pattern observed in the middle basin is of two surface gyres: cyclonic in the north and anticyclonic in the south (Tuzhilkin and Kozarev, 2005). The east coast shows a summer upwelling pattern due to prevailing north-easterly winds. Most **nutrients** enter the CS through the northern basin via the Volga River.

The bay of the Karabogaz, located on the shallow eastern coast, serves as an overflow for the CS (Giralt et al., 2003; Leroy et al., 2006). The Karabogaz Gol serves as an evaporator for the overflow water in the CS, and therefore is extremely saline.

The present CS level is at 26.5 m bsl (Naderi Beni et al., 2013). The still partial reconstruction of the Late Pleistocene and Holocene sea level history highlights a great complexity and has been summarised recently in Leroy et al. (2013c). The main authors, Klige (1990), Rychagov (1997), Chepalyga (2007) and Svitoch (2012) provide conflicting sea level curves for the Late Pleistocene and Holocene. The range of accepted changes is large, somewhere between > −100 m and +50 m. The maximal elevation is related to the altitude of the Kuma–Manych depression (26 m asl) and the lower Don River, which allow water outflow to the Black Sea.

2.3. Previous studies in the area

2.3.1. Open sea cores taken in the INCO-Copernicus project

In August 1994, cores from the south and middle basins were taken during a French–Russian oceanographic cruise (Table 1). All

Table 1
Names and location of some of the cores taken during the French–Russian expedition of 1994, presented or discussed here, and of a core from the S–E Caspian Sea, Iranian coast (see Fig. 1B for location map). NB: Core GS18 has also been called core GS20 in previous publications (Boomer et al., 2005; Tudryn et al., in press).

Name used here	Station no	On board no	Museum no core length	Latitude and longitude water depth
GS04	2	SR9402GS04	−787 cm	38°41′39″N, 51°36′36″E 405 m
GS05	2	SR9402GS05	SR01GS9405 957 cm	38°45′39″N, 51°32′16″E 518 m
CP14	6	SR9406CP16	SR01GS9414CP 140	39°16′18″N, 51°27′47″E 330 m
CP18	9	SR9409CP20	SR01GS9418CP 182 cm	41°32′53″N, 51°06′04″E 480 m
GS18	**9**	**SR9409GS20**	**SR01GS9418 995 cm**	**41°32′53″N, 51°06′04″E 479 m**
GS19	9	SR9409GS19	−925 cm	41°32′38″N, 51°06′06″E 478 m
CP21	11	SR9411CP23	SR01GS9421CP 170 cm	42°50′31″N, 49°51′17″E 460 m
Core name TM	Core length (cm) 2750 cm		Altitude 2 m above sea, i.e. −25.5 m	Latitude and longitude 37°09′06″N, 54°03′24″

cores were retrieved from deep basin locations, usually >400 m, to avoid direct river delta influence, guided by seismic profiles and seismic maps, but this information had unfortunately to remain secret (Fig. 1). With the aim of recovering complete sections for the Late Pleistocene and the Holocene, three coring techniques were combined. The Kullenberg cores, typically 10 m long, 90 mm of diameter, lost probably the upper c. 1 m of sediment at the moment of sediment penetration by the corer. The Pilot cores, c. 150–200 cm long, also lost a few upper decimetres during coring. Fortunately the Usnel box cores (c. 50 cm thick) contain the water–sediment interface (Leroy et al., 2013b).

Palynological studies for three short Holocene Pilot cores (cores CP14, CP18 and CP21, not older than 5.5 cal. ka BP) located from the south to the north of the CS, and for a long Kullenberg core in the south basin (core GS05 from >11.2 to 4.4 cal. ka BP) are already published (Leroy et al., 2007, 2013c) (Fig. 1); while the results of the

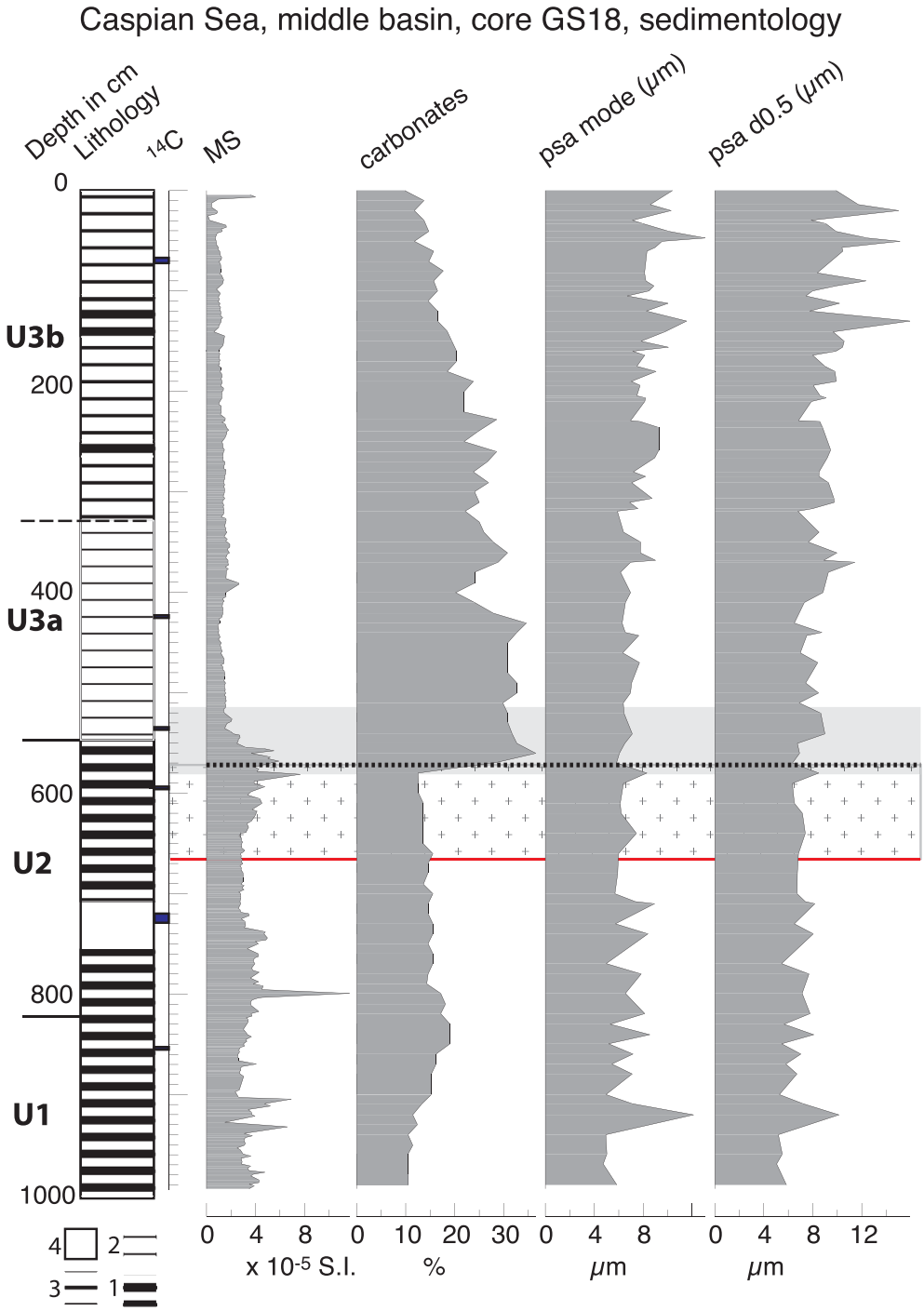

Fig. 2. Sedimentological data: lithology, location of ^{14}C samples, magnetic susceptibility (MS), carbonate content (after Chalié et al., 1997) and particle size analysis (psa) of core GS18. The horizontal dashed line shows the drop in particle size as defined by a zonation analysis. The horizontal box with crosses highlights the Younger Dryas stadial, and the light grey one the Mangyshlak lowstand, both events identified by the palynological analysis. The thin continuous horizontal line indicates where the palynological data start. Legend: 1) coarse lamination with dark layers, 2) fine lamination, 3) pale lamination, and 4) absence of lamination.

long core in the middle basin has not been published yet, being the object of the present work. The two pilot cores, CP18 and CP21, from the middle basin, could not be dated owing to the abundance of reworked carbonates (Leroy et al., 2007). The present study focuses on the Kullenberg core GS18 (also called GS20 in Boomer et al., 2005 and Tudryn et al., in press; Table 1) located in the middle basin.

2.3.2. Previous studies on long cores in the middle basin

2.3.2.1. Coring. Cores GS18 and GS19 are two Kullenberg cores taken in the same site, in the centre of the middle basin (Fig. 1, Table 1). Whilst the palaeoenvironmental analyses of core GS19 were published by the Russian partner in the INCO-Copernicus project (Kuprin et al., 2003), those of core GS18, especially palynology, have remained so far largely unpublished (Boomer et al., 2005; Tudryn et al., in press). In the south basin, previous studies performed on the Kullenberg cores GS04 (Kuprin et al., 2003) and GS05 (Leroy et al., 2013c) are used for comparison.

2.3.2.2. Lithology. The sediment of core GS18 generally is fine-grained. Boomer et al. (2005) differentiated three lithological units (Fig. 2). Unit 1, from 995 to 820 cm, consists of dark beige detrital and authigenic carbonate clays. The carbonate percentages start with values around 10. A temporary increase occurs to 19% towards the end of the unit (850-820 cm). The sediment is strongly laminated with, in general, a 2 mm dark lamina and a 5.3 mm light lamina.

After a progressive change, unit 2, from 820 to 552.5 cm, consists of light beige clays with detrital and authigenic carbonates (stable values around 13–14%). This unit is also strongly laminated except between 752 and 704 cm. The carbonates data indicate a major and rapid increase between 580 (12%) and 569 (30%) cm depth.

After a sharp change, unit 3a, from 552.5 to 326 cm, is a grey to green mud, with mostly detrital carbonates and some authigenic carbonates. Laminations are almost absent. In unit 3b (326 cm to top), the sediment is a grey to green mud, mostly made of detrital carbonates, with rare authigenic carbonates. The laminites are first faint and then become more strongly visible at 263–250 and 145–103 cm depth. The carbonate content of unit 3 starts first with maximal values at > 35% and then decreases progressively down to 10%.

Similarly, core GS19 shows a fine-grained laminated sediment without disturbances (Kuprin et al., 2003). A major change in lithology at 642 cm is marked by a similar increase of carbonates as that observed in core GS18 at 580-569 cm depth.

2.3.2.3. Dating of cores GS18 and GS19 and palaeo-environmental reconstructions. In Boomer et al. (2005), the results of investigations of ostracod assemblages and carbonates from core GS18 based on a chronology made from three radiocarbon dates on ostracod shells were presented. The main results are that the bottom waters have remained ventilated, which allows the existence of an ostracod fauna. Also a main change at the Pleistocene/Holocene transition has been recognised with a sharp increase of Loxoconchidae at c. 580 cm depth. In the later publication of Tudryn et al. (in press), the number of ^{14}C dates was increased to six, and the magnetic properties of the sequence were discussed at laminae scale. It was shown that lamination is due to alternation of greigite, an early diagenetic iron sulphide, and detrital magnetite, an iron oxide. Rhythmic changes of these minerals reflect changes in the oxygenation of the sea bed, with phases of good and restricted ventilation, even if the sediment bottom was never totally depleted in dissolved oxygen (Boomer et al., 2005).

The sequence of **core GS19** is dated by nine radiocarbon dates on bulk sediment (Ferronsky et al., 1999). The authors indicate that these dates have to be corrected by 10–20% due to dead carbon. In combination with the sedimentological study Kuprin et al. (2003) interpreted a low stand in the Late Khvalynian at 642–582 cm (with a non-corrected bulk ^{14}C date of 11.3 ka BP at 600 cm). However this period was not formally related to the Mangyshlak lowstand. It is followed by a transgression from 582 to 486 cm depth. A regression took place between 486 cm (shortly before a non-corrected bulk ^{14}C date of 9.6 ka BP at 470 cm) and 414 cm (earlier than a non-corrected bulk ^{14}C date of 8.86 ka BP at 410 cm) attributed to the Early Neocaspian. The main results of the very preliminary pollen analyses made on this core (23 samples and 12 taxa) (Kuprin and Rybakova, 2003) suggest that transgressions took place during periods of cool and humid climate with forest expanded into present day semiarid areas.

3. Material and methods

3.1. Radiocarbon dating, grain size and magnetic susceptibility

Six radiocarbon dates were obtained from ostracod shells (Tudryn et al., in press). These radiocarbon ages have been used to build an age–depth model after applying a 370 years reservoir effect (as in Leroy et al., 2013c) and calibration using the IntCal13.14C curve (Reimer et al., 2013) (Table 2). The age–depth modelling has been performed here using Clam.R 2.2 (Blaauw, 2010). A good fit was provided by a smooth spline solution with a smooth factor of 0.3 (Fig. 3).

New particle size analyses of 92 samples were made by laser granulometry on bulk sediments using a Coulter LS 130 instrument. D0.5 is the median. Additionally, 375 new low field magnetic susceptibility measurements were obtained on U-channels with a Bartington MS-2 susceptibility meter. A CONISS zonation has been applied on the four curves (Fig. 2).

3.2. Palynological analyses

Ninety-two samples for the top 666 cm of core GS18 were palynologically studied. Twenty-two of them were treated at UCL

Table 2
Radiocarbon dating results for core GS18. Radiocarbon ages were calibrated using the IntCal13.14C calibration (Reimer et al., 2013) and a 370 yr reservoir effect was considered (Leroy et al., 2013c).

Mean depth (cm)	Depth interval (cm)	Laboratory code	Dated material	^{14}C age (yr BP)	± (yr BP)	Calibrated 2σ (cal. yr BP) and 370 yr reservoir effect
69.5	72–67	Poz16737	Ostracods	3550	35	3345–3470
424.5	427–422	GifA100565	Ostracods	8300	140	8430–9127
535.5	538–533	GifA100566	Ostracods	9960	120	10,592–11,214
595	597–593	GifA100567	Ostracods	10,610	130	11,402–12,511
725	730–720	Poz16738	Ostracods	11,330	60	12,716–12,983
853	854–851	Poz16739	Ostracods	12,260	60	13,553–13,934

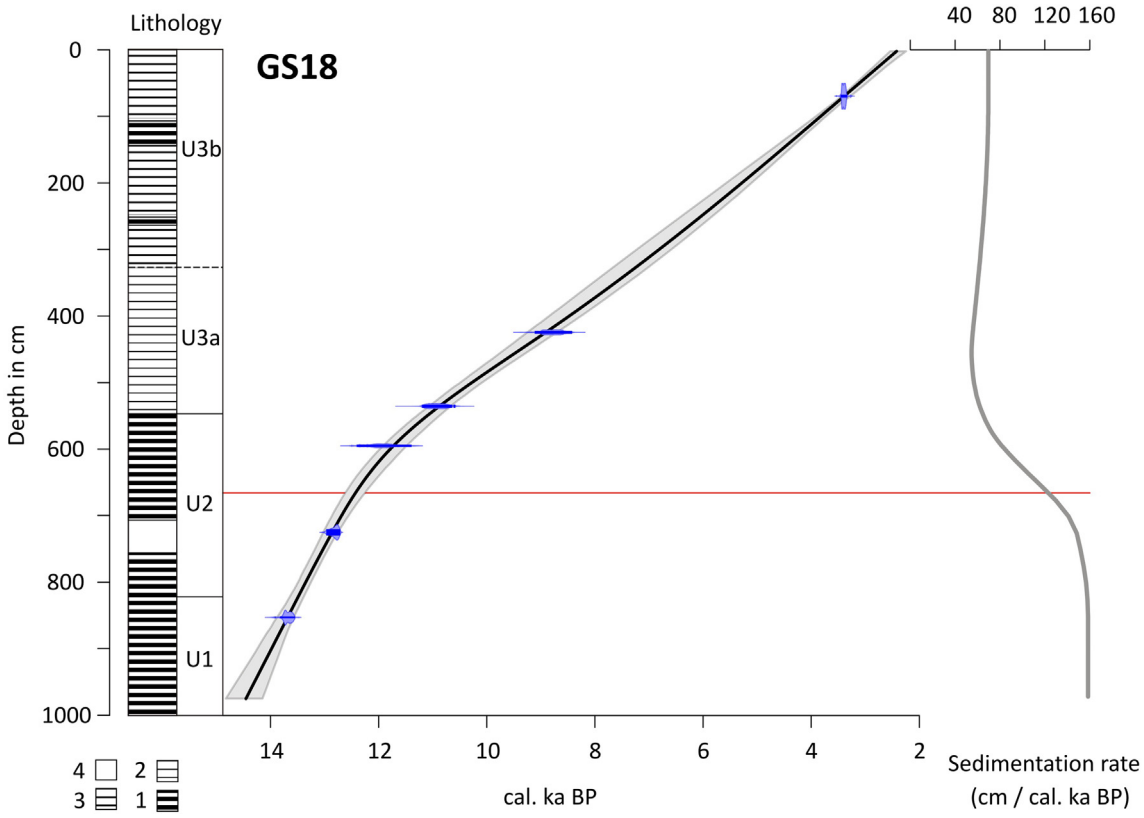

Fig. 3. Age–depth model and sedimentation rates for core GS18. Lithological symbols and red horizontal line as in Fig. 2. (For interpretation of the references to colour in this figure legend, the reader is referred to the web version of this article.)

(Belgium) by the heavy liquid method (Thoulet solution at a density of 2.1). The remaining seventy samples were treated at Brunel University (UK) by the HF method. On average the sample volume was 1.1 ml. Initial processing of samples involved the addition of sodium pyrophosphate to deflocculate the sediment. Samples were then treated with cold hydrochloric acid (10%) and cold hydrofluoric acid (32%), and HCl again. The residual organic fraction was screened through 125 and 10 μm mesh sieves. Final residues were mounted on slides in glycerol and sealed with varnish. *Lycopodium* tablets were added at the beginning of the process for concentration estimation in number of pollen and spores per ml of wet sediment (without the non-pollen palynomorphs or NPP), but only in the samples treated at Brunel University; for the rest no concentration estimates are available. The use of two different palynological methods to treat the samples did not bias the recovery of dinocysts (see Supplementary Information for more information).

An additional 22 samples, below 666 cm depth, were treated but not considered here because of i) the irregular presence of high percentages of *Pinus* pollen (probably reworked or river transported), ii) the very high occurrence of reworked pollen grains (loss of ornamentation, increase in opacity and often pre-Quaternary taxa), and iii) the very low palynological concentrations (below 2000 pollen and spores per ml). This jointly points to a different taphonomy than for the upper part of the core.

For the section above 666 cm, the average pollen sum is 364, considering only terrestrial taxa. Dinoflagellate cysts were counted in the same slides. The average of counted cysts is 490, reaching below 100 cysts in only one case. The taxonomy and the ecological preferences of the CS dinocysts are detailed in the paper of Marret et al. (2004). Identifications of the dinocysts are based on Marret et al. (2004), Mertens et al. (2009), Leroy (2010) and Mudie et al. (2011). The cysts of *Lingulodinium machaerophorum* have processes of various shapes and lengths, which have been counted separately (following form names defined in Leroy et al., 2006).

The data were plotted in diagrams using Psimpoll (Bennett, 2007). The P/D ratio is the ratio of the concentration of pollen over dinocysts (McCarthy and Mudie, 1998).

3.3. Numerical methods

Zonation by cluster analysis (CONISS), after square root transformation of the percentage data, was calculated separately for pollen and spores (22 taxa) and for dinocyst (9 taxa) datasets using Psimpoll.

Multivariate techniques were applied to the datasets in order to detect and summarise the major patterns of variation of the data in few dimensions. An exploratory detrended correspondence analysis (DCA) on the pollen (excluding aquatics and NPP) and dinocyst datasets separately was first performed to provide information on the gradient length. As the gradients in both datasets were <2.5 SD, principal component analysis (PCA) was applied (Birks et al., 2012). Additionally, non-metric multidimensional scaling (NMDS) was also performed, and the results were not significantly different than those obtained after DCA and PCA. Hence, PCA was performed on pollen, excluding aquatics and NPPs, and dinocysts datasets separately. PCA explorations were made on the variance–covariance matrices, with the percentage data square root transformed prior to analysis. For pollen data, only those taxa with a significant presence were considered, and sums of trees (excluding Pinaceae) and shrubs were also incorporated. All dinocyst taxa from core GS18 have been included in the PCA together with data from the nearby CP18 core (Leroy et al., 2007) in an attempt to identify a possible

overlap between the two cores, as core CP18 does not have a chronology. *Spiniferites cruciformis* forms (A, B and C) identified in core GS18 were summed because in core CP18 no distinction between them was made due to their very low abundance. PCA was performed using the open software PAST 3.01 (Hammer et al., 2001).

4. Results and interpretation

4.1. Age–depth model and lithology

The age–depth model indicates that the sediment core spans between 14.47 and 2.43 cal. ka BP, and that the palynological data (the top 666 cm) provides information from 12.44 to 2.43 cal. ka BP (Fig. 3). The sedimentation rate is very high being c. 160–130 cm/cal. ka BP below 666 cm depth. It decreases above this depth, until its stabilisation with values of c. 75–55 cm/cal. ka BP (Fig. 3) reflecting the critical loss of the detritics brought by meltwater. The time resolution between palynological samples is on average 99 years.

Analyses in core GS18 show that the fine silty fraction is dominant throughout the sediment. The mean grain size value is 19.4 ± 13.5 μm, the mean mode value is 7.5 ± 1.6 μm and the mean median value is 8.4 ± 2.1 μm. Nevertheless, minor changes are observed (Fig. 2): a progressive grain size increase is recorded from the bottom to the top, as it is observed in the mode and median and for mean grain size, which corresponds to 9.4 (±2.8) μm for unit 1, to 18.5 (±17.9) μm for unit 2, to 19.5 (±10.2) μm for unit 3a and to 23.1 (±13.4) μm for unit 3b.

Magnetic susceptibility (Fig. 2) shows higher values in units 1 and 2, and lower values in the upper part of the sequence, with unit 3, reflecting a decrease in the magnetic minerals content. Indeed, units 1 and 2 are characterised by relatively important contents of ferrimagnetic iron minerals: early diagenetic greigite and detrital magnetite, changing rhythmically at laminae scale (Tudryn et al., in press). Greigite content variation dominates the magnetic susceptibility signal that shows some important peaks, such as c. 800 cm. Such large-amplitude peaks related to changes in greigite contents are also observed in the Late Pleistocene sediment from South Caspian Sea basin (Jelinowska et al., 1998, 1999). The decrease of magnetic susceptibility in unit 3 is due to the disappearance of the greigite that is replaced by paramagnetic pyrite. Pyrite, as greigite, is of early diagenetic origin and is related to the anoxic, sulphate-reducing conditions in the sediment. Its presence instead of greigite suggests a decrease of the Fe/S ratio in the environment, which can be due either to the increase of the water salinity or to the decrease of the availability of the iron due to the decrease of the detrital input to the lake.

4.2. The pollen, spores and non-pollen palynomorphs records

The zonation of the terrestrial signal by means of cluster analysis has distinguished six pollen zones from p-1 to p-6 (Fig. 4).

4.2.1. Zone p-1, 666-571 cm, 12.44–11.42 cal. ka BP: a very dry Younger Dryas

This zone contains the highest values of *Elaeagnus* and *Hippophae*, with a sub-continuous curve of *Picea* (Fig. 4). Other important taxa within the arboreal taxa (AP) are *Pinus* (10%) and *Quercus* (5%), the latter especially in the second half of the zone. Shrubs such as *Ephedra* and *Calligonum* are present, but not with large values. Amongst the non-arboreal pollen (NAP), Amaranthaceae dominate and also reach their maximal values (often > 50%). *Artemisia* is abundant, as well as Poaceae. It is also worth mentioning the occurrence of salt-tolerant plants such as Plumbaginaceae, *Haplophyllum* and *Nitraria*. Reworked pollen grains are relatively high, often >15%. *Radiosperma* is frequent in this zone only. Pollen concentrations are very low, around 3000 pollen and spores per ml of wet sediment.

The reconstructed Younger Dryas vegetation around the CS is a desert with some shrubs in the plains and some spruce in the Caucasus Mountains.

4.2.2. Zones p-2 to 4, 571–382.75 cm, 11.42–8.19 cal. ka BP: Early Holocene: dry shrubs onland but freshwater indicators

These three zones (p-2: 571–528 cm or 11.42–10.77 cal. ka BP, p-3: 528–439 cm or 10.77–9.19 cal. ka BP and p-4: 439–382.75 cm or 9.19–8.19 cal. ka BP) have many common points, but also show some differences. They all have rather high percentages of *Pinus* (up to 30% in some samples). *Picea* is still frequent, but not later on. The main feature of these three zones is the shrub maxima: first *Calligonum*, then *Ephedra major*-t. (or *distachya*-t.) and then *Ephedra alata*-t. (or *fragilis*-t.). In the AP, *Corylus* peaks in zone p-2. *Quercus* percentages, after a brief decrease in zone p-2, carry on increasing. *Tilia* becomes more frequent from zone p-4 onwards.

In the NAP, Caryophyllaceae, Ericaceae, Rubiaceae and Plumbaginaceae are frequent. Although *Artemisia* and Amaranthaceae are the main taxa, their values are lower than in the zone p-1, especially in zone p-2. Spores of ferns are more frequent, while reworked pollen values decrease in these three zones. Concentrations are still low, i.e. mostly less than 8000 pollen and spores per ml of wet sediment.

Another characteristic of these zones is the rather abrupt development of the cyanobacteria *Anabaena* from zone p-2 and of the green algae *Botryococcus* from zone p-3, both until the end of zone p-4. *Pediastrum* is slightly more frequent than in zone p-1. Incertae Sedis 5b (a probable green algae) show a progressive increase peaking in zone p-4. A few leaf spines of the aquatic plant *Ceratophyllum* are noted especially in zone p-3. Massulae of the floating fern *Salvinia* start to occur in zone p-4. Many of these NPPs indicate lenses of freshwater at the surface of the CS, especially in zones p-3 and 4, perhaps owing to precipitation and/or to long-distance hypopycnal flows from the west. A similar explanation was proposed for the Aral Sea mixed micropalaeontological assemblages (Sorrel et al., 2006).

The inferred environment at the beginning of the Holocene is an open landscape with many shrubs, possibly on sand dunes (which must have been more widespread than nowadays as the vegetation cover was less dense than today), and some scattered trees in limited favourable areas. Some freshwater indicators are found either derived from the coast of the CS or from its surface. It is suggested that rivers were active.

4.2.3. Zone p-5, 382.75–76.25 cm, 8.19–3.50 cal. ka BP: Middle Holocene, first deciduous tree development

Although Amaranthaceae values are maximal and *Artemisia* percentages also increase, this rather long pollen zone shows the development of several deciduous trees: *Salix*, *Tamarix*, *Ulmus–Zelkova*, *Carpinus betulus*, *Quercus*, *Corylus*, *Tilia* and the vine *Vitis*. Two occurrences of *Pterocarya* are noted at the beginning and at the end of this zone. Pollen and spores concentrations are tenfold higher than in earlier periods. Algal remains are abundant although less than in the previous zone (p-2 to p-4). *Tetraedron* is now common. Incertae Sedis 5d (another probable green algae) starts to become frequent.

The reconstructed vegetation for the Middle Holocene is a semi-open landscape with the development of a steppe, but retaining many desertic areas. Trees are more abundant and diverse, but still only in limited areas with higher precipitation, such as the Caucasus and the Elburz Mountains.

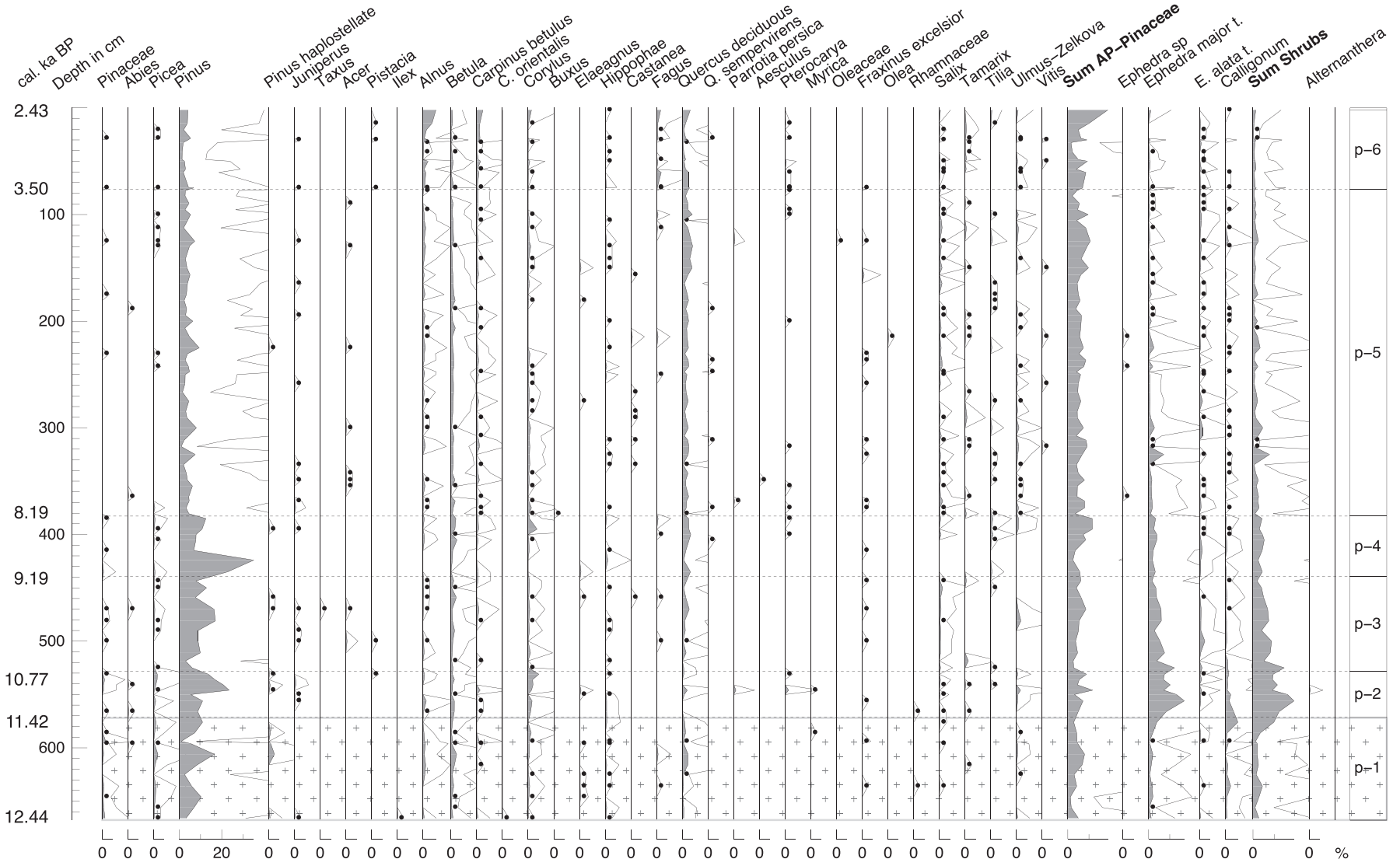

Fig. 4. Pollen and spore diagram of core GS18. The horizontal box with crosses highlights the Younger Dryas stadial. 10X exaggeration curves and dots for values lower than 0.5%.

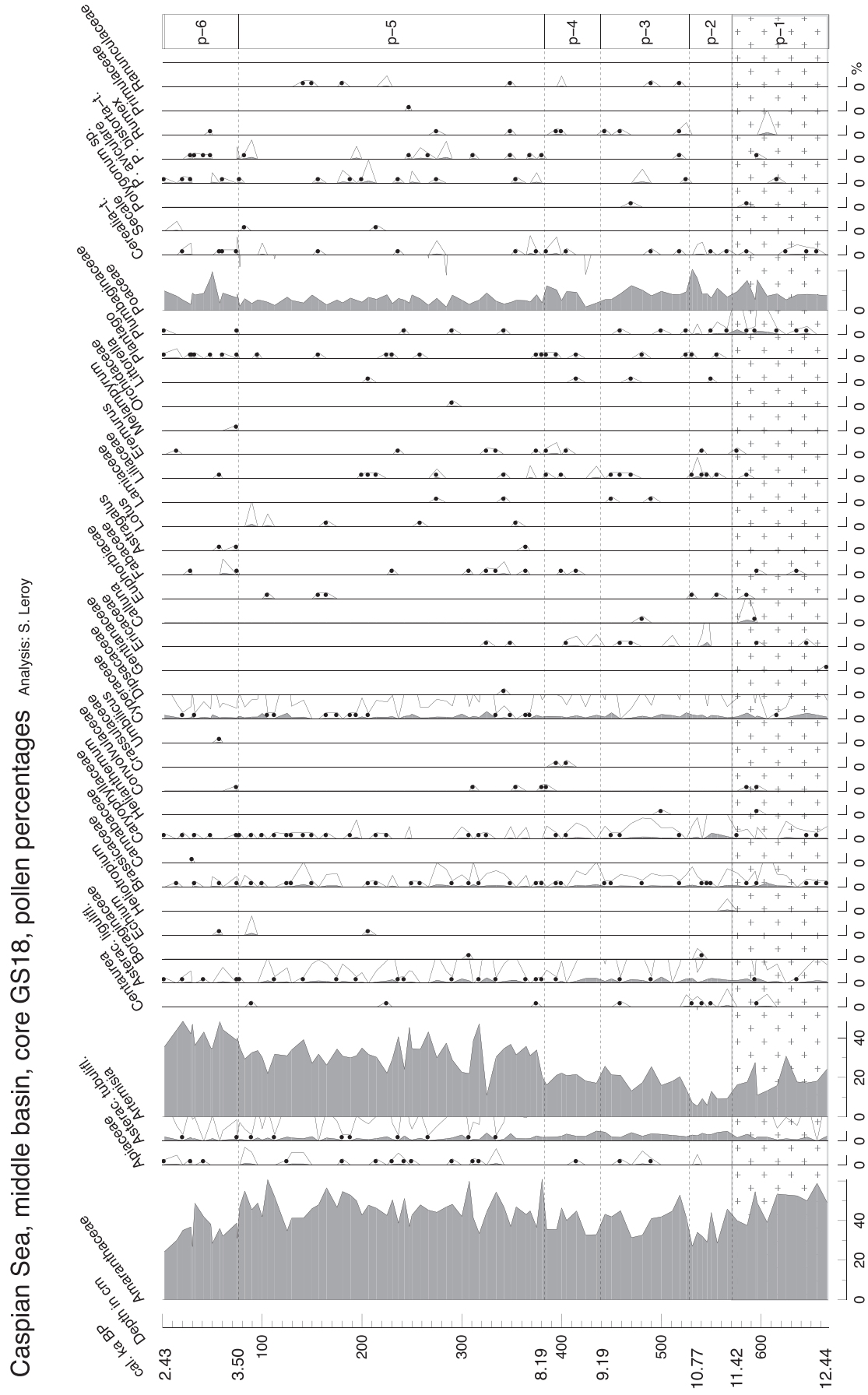

Fig. 4. (*continued*).

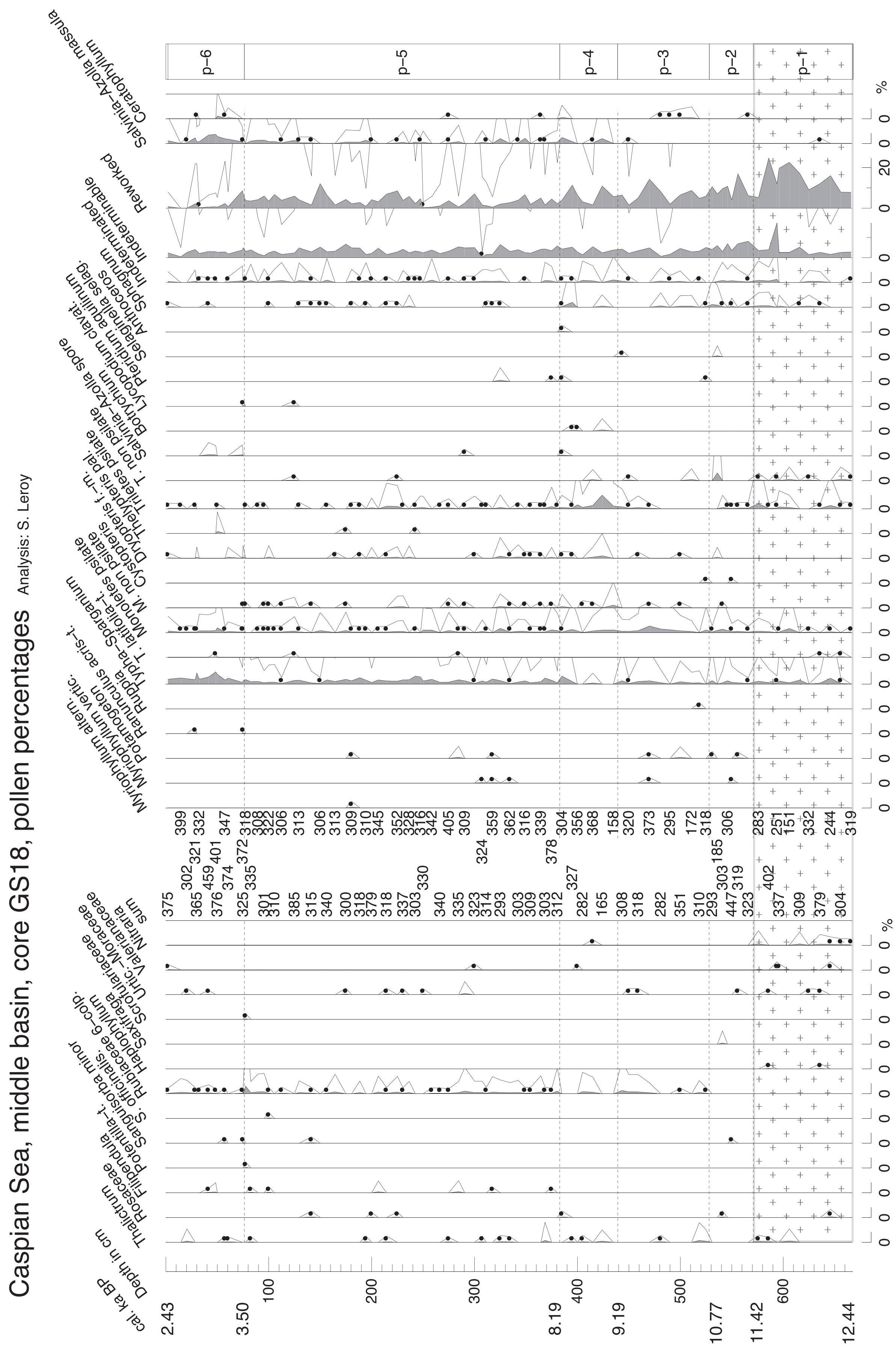

Fig. 4. (*continued*).

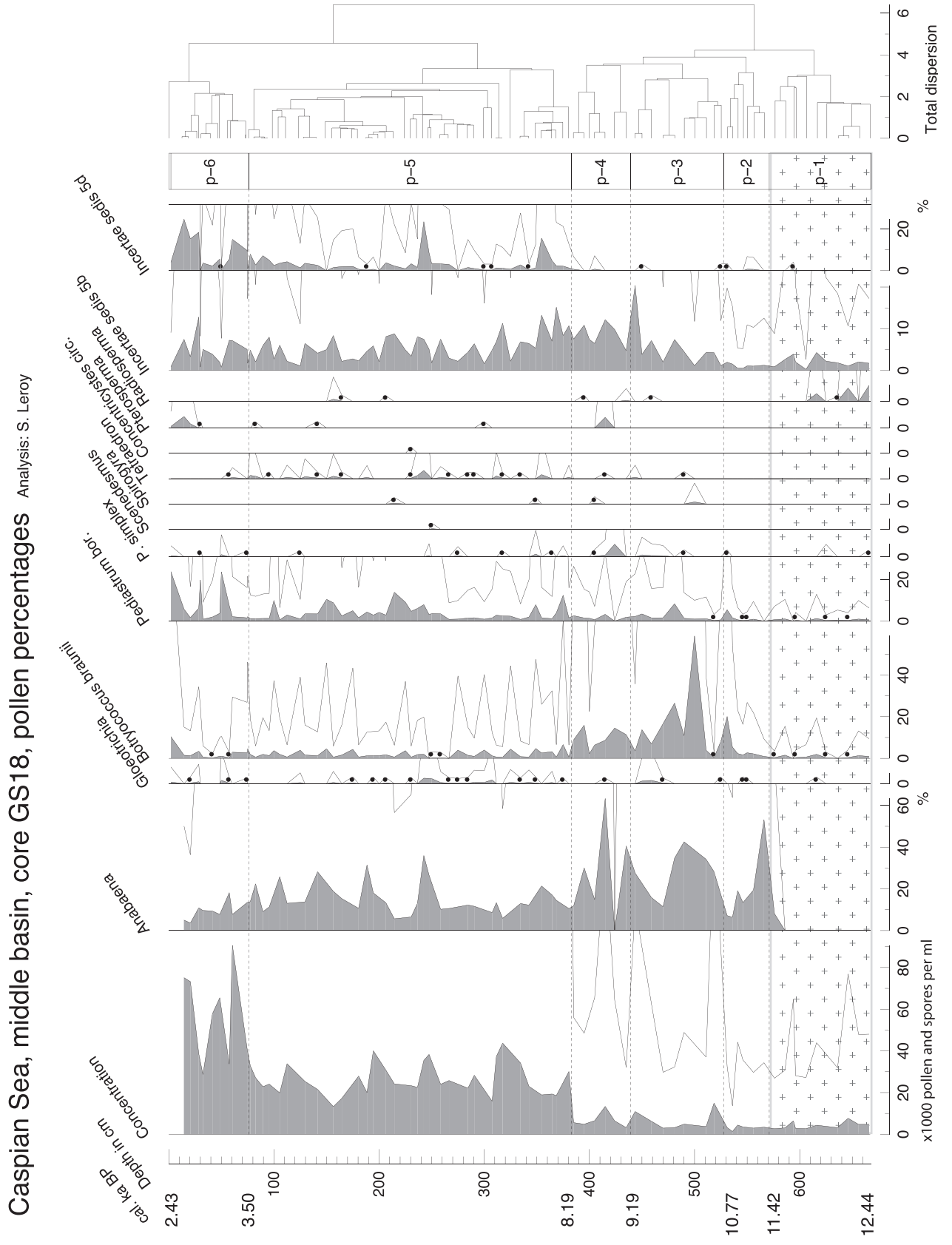

Fig. 4. (*continued*).

4.2.4. Zone p-6, 76.25 cm to top, 3.50–2.43 cal. ka BP: Late Holocene, further deciduous tree increase

This zone is characterised by a further increase of deciduous trees, mainly *Alnus*, *C. betulus*, *Fagus* and *Pterocarya*. The values of Amaranthaceae drop, while *Artemisia* reaches a maximum, indicating the advance of the steppe. *Plantago* and Poaceae reach a maximum, as well as *Typha–Sparganium*, *Salvinia* massulae and Incertae Sedis 5d. Pollen concentrations are maximal, mostly between 40,000 and 80,000 pollen and spores per ml. Occasionally *Pediastrum* reaches values up to 20%. *Pterosperma* is frequent, but in the last samples only.

The Late Holocene is characterised by a replacement of the desert by a steppe in many places, and the arboreal component is the most abundant and diverse of the whole sequence.

4.3. The dinocyst record

The zonation of the aquatic signal by means of cluster analysis has allowed distinguishing five dinocyst zones from d-1 to d-5 (Fig. 5).

4.3.1. Zone d-1, 666-581 cm, 12.44–11.56 cal. ka BP: Khvalynian highstand with Spiniferites belerius

This zone contains a maximum of *Pyxidinopsis psilata* values and increasing values of *S. cruciformis* (Fig. 5). *S. belerius* is also present and it is a characteristic of this zone only. Very low dinocyst concentrations are observed, in the range of 3000 specimens per ml.

A highstand, attributed to the Khvalynian, is reconstructed based on similarities with the dinocyst assemblages i) in the Black Sea during the periods of high meltwater influx (Wall and Dale, 1973) and ii) at the base of core CP14 (Leroy et al., 2007).

4.3.2. Zone d-2, 581–419.5 cm, 11.56–8.83 cal. ka BP: the Mangyshlak lowstand followed by a highstand

Overall zone d-2 has a low P/D ratio. From this zone onwards, the concentrations are satisfactory in the order of 20,000 cysts per ml. An important change, not highlighted by the cluster analysis, occurs at 515 cm or 10.55 cal. ka BP.

Subzone d-2a (581–515 cm, 11.56–10.55 cal. ka BP) is characterised by high values of *Impagidinium caspienense* and low values of *S. cruciformis*. The similarity to the modern CS assemblages suggests relatively higher salinities than previously, which are related here to the Mangyshlak lowstand as in core GS05 (Leroy et al., 2013c).

Subzone d-2b (515–419.5 cm, 10.55–8.83 cal. ka BP) contains both *P. psilata* and a maximum of *S. cruciformis*. This subzone is interpreted as indicative of a new period of highstand, similar to that reconstructed in zone d-1.

4.3.3. Zone d-3, 419.5–329.75 cm, 8.83–7.30 cal. ka BP: drop of S. cruciformis

This zone shows abundant *P. psilata* but a sharp drop of *S. cruciformis* in comparison to zone d-2b. A slowly increasing ratio of P/D is observed.

4.3.4. Zone d-4, 329.75–18.75 cm, 7.30–4.11 cal. ka BP: a slow regression

P. psilata percentages fluctuate with a brief, but pronounced drop at the beginning of this subzone. Nevertheless, its percentages have a decreasing trend; while high values of *Brigantedinium* start to occur, which carry on to the diagram top. *I. caspienense* shows a slight increase trend. The P/D ratio reaches moderate values of 15–20.

4.3.5. Zone d-5, 118.75 cm to top, 4.11–2.43 cal. ka BP, Neocaspian intermediate levels

This zone may be subdivided into two parts, at 24.5 cm or 2.75 cal. ka BP.

Subzone d-5a (118.75–24.5 cm, 4.1–2.75 cal. ka BP) presents important changes in the dinocyst assemblages with the quasi disappearance of *P. psilata* and the very low values of *S. cruciformis* reduced to its form A (Marret et al., 2004). Maxima of *I. caspienense* and *Pentapharsodinium dalei* cysts occur, but *Caspidinium rugosum rugosum*, with values quasi constant during the previous zones, almost comes to an end. A very high P/D ratio is observed, often above 30.

Subzone d-5b (24.5-top, 2.75–2.43 cal. ka BP) also shows very high values of *I. caspienense*. Hardly any *P. psilata* and *S. cruciformis* are noted. *L. machaerophorum* clearly starts to develop. High values P/D are still recorded.

Zone d-5 is interpreted as reflecting the intermediate levels of the Neocaspian period due to the high values of *I. caspienense*. Core GS18 assemblages in this zone are similar to those of core CP18 (Leroy et al., 2007). The development of *L. machaerophorum* in subzone d-5b is interpreted as reflecting a slight warming trend of the waters and it is typical of the last millennia in most Caspian cores (Leroy et al., 2013b).

4.4. PCA of the terrestrial and aquatic signals

For the terrestrial signal (pollen) of core GS18, two principal components had eigenvalues above the broken stick values. The first principal component (PC1-p) accounts for 44.7% of the variance, while the second principal component (PC2-p) explains 12.1%. In **PC1-p**, the sum of shrubs, *E. major* t. and *Pinus* present high positive loadings, while *Artemisia* has a very negative loading (Fig. 6). This principal component shows factor scores close to zero during zone p-1, positive from zone p-2 to zone p-4, and mostly negative in zones p-5 and p-6 (Fig. 7), thus, pointing to a shrub phase from 11.42 to 8.19 cal. ka BP. In **PC2-p**, the sum of trees (excluding Pinaceae), several mesophytes (*Alnus*, *C. betulus*, *Quercus*) and Poaceae show positive loadings, while Amaranthaceae have a very negative one (Fig. 6). This component has negative scores in zone p-1, close to zero from zone p-2 to p-5, and positive ones in zone p-6. PC2-p is related to mesophytic forests versus saline habitats.

For the aquatic signal (dinocysts) of cores GS18 and CP18, the two first principal components are also significant. The first one (PC1-d) explains 68% of the variance, while the second one (PC2-d) accounts for 16.2%. In **PC1-d**, *P. psilata* and *S. cruciformis* show positive loadings, while *I. caspienense* and *L. machaerophorum* have negative ones (Fig. 6). This component, thus, presents a salinity gradient. Samples with positive factor scores reflect low salinity waters, while samples with negative scores point to higher salinities. Factor scores are positive from zone d-1 to d-4 in core GS18, although slightly closer to zero in zone d-2a and with a decreasing trend in zone d-4; while at 4.11 cal. ka BP an abrupt shift occurs and scores become negative in zone d-5. Scores are always negative in core CP18 (Fig. 7). In **PC2-d**, *Brigantedinium* presents a very negative loading, while *L. machaerophorum* has a positive one (Fig. 6). In core GS18, scores are always close to zero, although slightly positive in zones d-1 and d-2, slightly negative from 8.83 cal. ka BP in zones d-3 to d-5a, and mostly positive again from 2.75 cal. ka BP in zone d-5b. For core CP18, scores are close to zero at the bottom but with an increasing trend at the upper part (Fig. 7). We hypothesise this principal component as reflecting changes in river origin (see Discussion).

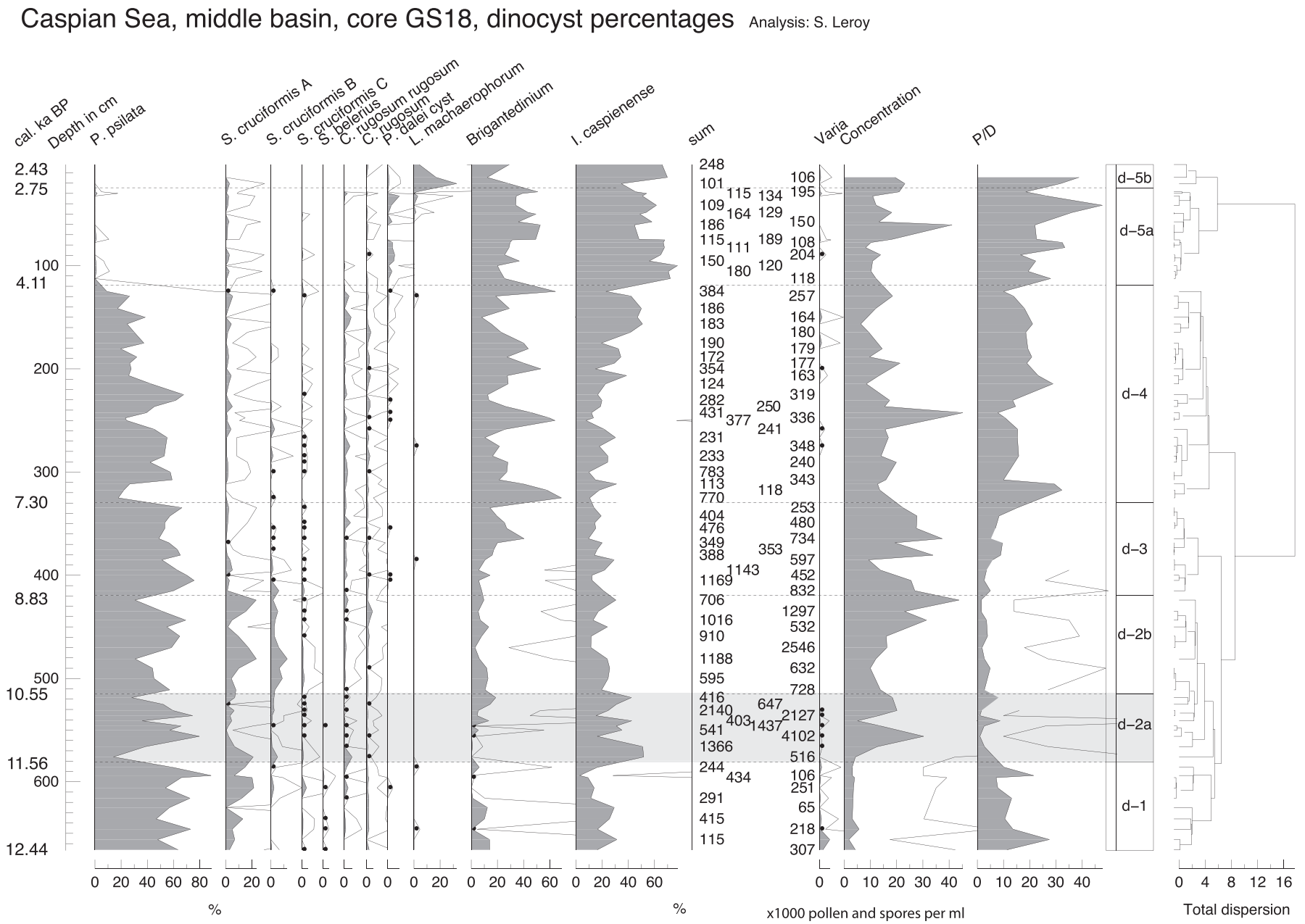

Fig. 5. Dinocyst diagram of core GS18. The horizontal grey box highlights the Mangyshlak lowstand. 10X exaggeration curves and dots for values lower than 0.5%.

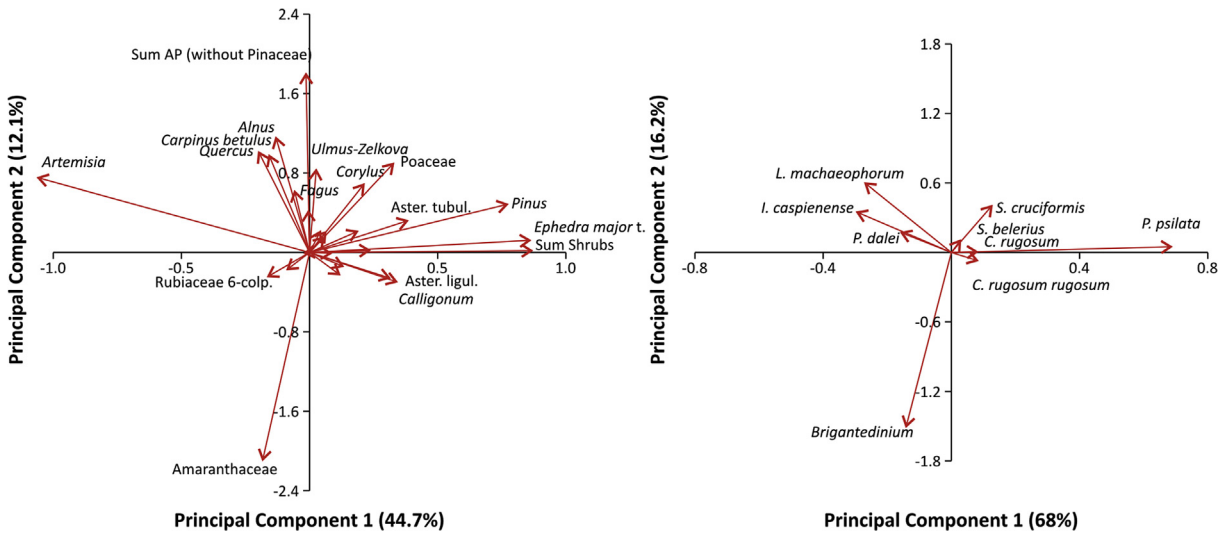

Fig. 6. Loadings plot (eigenvalue scale) of the two principal components for the terrestrial (left, pollen – only the names of the taxa with high loadings are included) and lacustrine (right, dinocysts) taxa included in the two PCA made in this study. For pollen, data are from GS18 core; while for dinocysts, data are from cores GS18 and CP18.

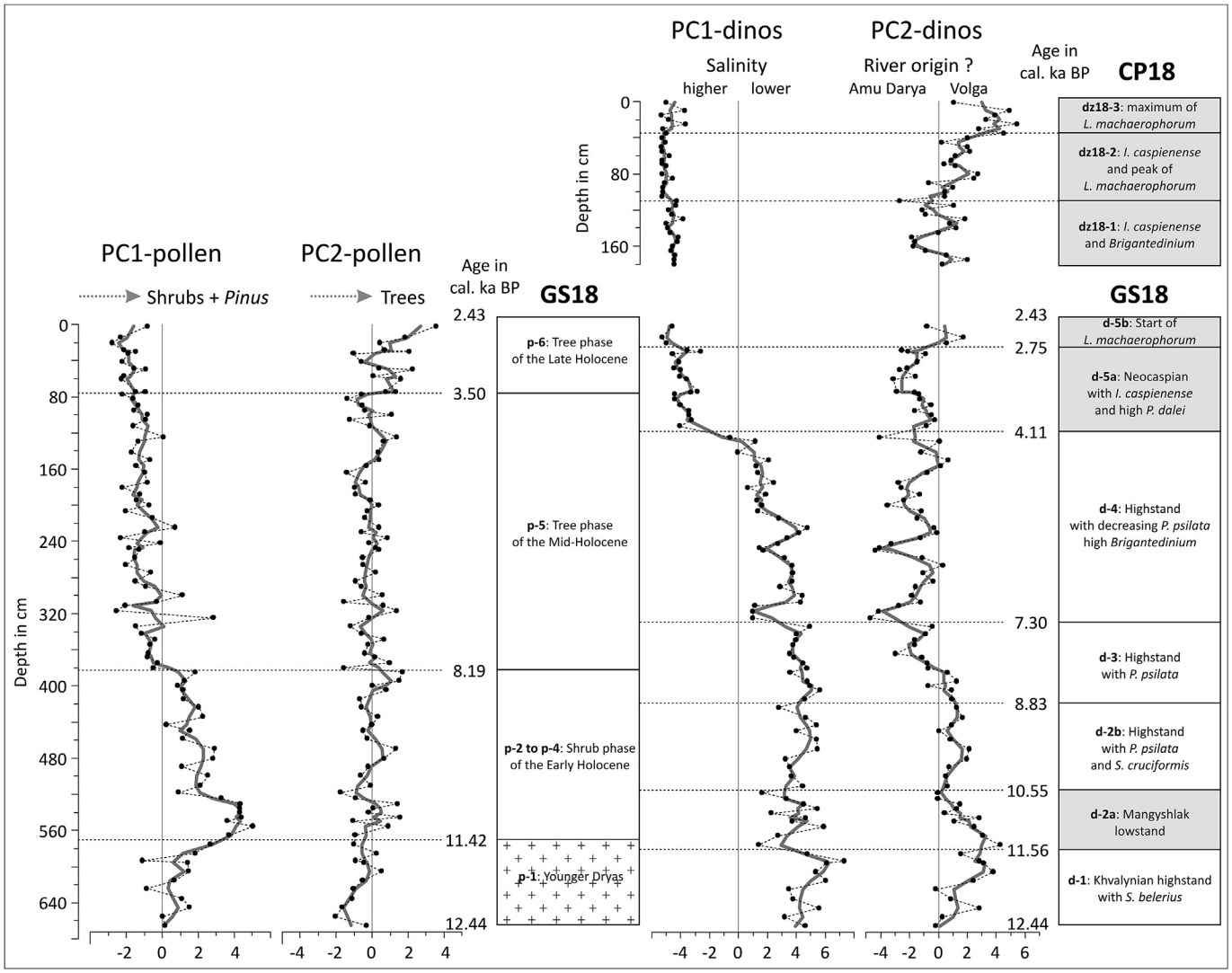

Fig. 7. Factor scores for the significant principal components obtained in this study and comparison of the pollen and dinocysts zonations Left: Results of the PCA on the GS18 pollen data. Right: Results of the PCA on the GS18 and CP18 dinocyst data. A 3-sample running average has been added to each graph.

5. Discussion

5.1. Age–depth model and correlation between GS18 and CP18 cores

Several Holocene palynological sequences may be compared in the CS. Their age–depth models were obtained using different approaches. The radiocarbon dates of core TM (SE corner of the CS) come from various shells with a 410 yr reservoir correction (Marine09) (Leroy et al., 2013a), the dates on core GS05 (middle of south basin) are from bulk sediment corrected from their detrital carbonate amount (with a reservoir of 370 yr) and calibrated with the IntCal09.14C curve (Leroy et al., 2013c), and finally those of core GS18 are from benthic ostracod shells, in which a reservoir effect of 370 yr was considered and the calibration was performed with the IntCal13.14C curve. The chronology of the short core CP14 was obtained based on a radiocarbon chronology, with a complex correction of the ages from the detrital carbonates and water ages, whereas no chronology was proposed for the short core CP18 because of the too high content in detrital carbonates that precludes corrections (Leroy et al., 2007). As mentioned earlier, the chronologies of cores GS04 and GS19 were based on radiocarbon dates on bulk sediment without correction. Hence, a wide range of dated material, corrections and age–depth models co-exists, illustrating the difficulty of working on Caspian material.

Cores CP18 and GS18 are both in the same coring station 9. Based on visual sediment description, carbonate contents, the first appearances of *L. machaerophorum* and *Pterosperma*, and the PC1-d and PC2-d scores, an overlap between the top of core GS18 (zone d-5b) and the bottom of core CP18 (zone dz18-1) is very likely (Figs. 3–5 and 7). The *Lingulodinium machaeorophorum* percentages' increase is a common feature for the Late Holocene in the CS dinocyst records (Leroy et al., 2013b). The *Pterosperma* increase is also observed in the three Holocene pilot cores (Leroy et al., 2007). When compared to the CP18 pollen diagram (Leroy et al., 2007), the decrease of Amaranthaceae and increase of *Artemisia* in zone GS18 p-6, i.e the development of the steppe, extend to pz18-1. In conclusion, approximately 35–95 cm of overlap may be suggested and a minimum of 85–145 cm seems to be missing at the top of core GS18 due to coring loss.

5.2. Vegetation history

The vegetation history reconstructed in sequence GS18 (middle basin) is fairly similar to that of sequences GS05 and TM (south basin) (Fig. 1). A comparison of the two deep basin cores, GS05 and GS18, indicates similar timing for the end of the Younger Dryas (11.5 versus 11.4 cal. ka BP), a period with a notable presence of *Elaeagnus* and *Hippophae* in both cores and reconstructed as cold and dry. A notable phase, well identified by the PCA (Fig. 7; and Fig. 5 in Leroy et al., 2013c), in which shrubs notably developed, occurs from the beginning of the Holocene to 8.4 and 8.2 cal. ka BP for GS05 and GS18 respectively. From that point onwards trees became more important and shrubs lost their Early Holocene hegemony. Thus, the two cores have a common feature that is the delay in the tree development of more than three millennia after the Holocene onset. Further steps in tree expansion occurred after 8.4–8.2 cal. ka BP, being more evident in core GS05 than in GS18. The next step happened at 3.5 cal. ka BP in core GS18 and at 3.9 cal. ka BP in the pilot core CP14 close to GS05 (Leroy et al., 2007).

Interestingly, the GS18 pollen record shows higher percentages of *Pinus*, *Ephedra*, Ericaceae, Poaceae and *Hippophae*, but slightly lower values of deciduous trees and *Nitraria* than the GS05 record. This reflects the existing gradient in precipitation, which decreases from the south to the north and makes arboreal formations more important on the Iranian coast (seen in the south basin core GS05), and desert/steppe formations more abundant at the higher latitudes reflected in core GS18 in the middle CS basin. The eastern Caucasus is probably the main source for arboreal pollen in core GS18. It was also a refugium for cold-loving trees during the Last Glacial Maximum (Leroy and Arpe, 2007; Arpe et al., 2011). An endemic species of the Elburz Mountains, *Parrotia persica*, is found in the diagram of GS18 indicating a clear southern component by air transport. In the south CS coastal in core TM, arboreal percentages are higher than in cores GS05 and GS18 and reflect the importance of forests due to its proximity to the Elburz Mountains, an area with a wide variety of habitats, that was a glacial refugium for a wide range of species (Leroy and Arpe, 2007; Arpe et al., 2011).

Contrary to the pollen interpretations made on core GS19 (Kuprin and Rybakova, 2003), no direct link was found between transgressions and widespread forest cover in the more detailed diagrams of core GS18. This is because the present investigation was able to separate onland changes from those in the water body. Broader comparisons can only be made to a few other diagrams, due to the scarcity of regional palynological studies. Forest started to appear slowly in Lake Aligol (southern Georgia, Caucasus), more than 590 km away from core GS18 (A in Fig. 1A), about 11.5 cal. ka ago. An important phase of *Ephedra distachya*-t. (>40%) is noticeable until c. 11 cal. ka BP. The real forest expansion was, however, delayed until 4.5 cal. ka BP, the suggested cause in this case being human activities (Connor, 2006). The Holocene part of the Lake Urmia sequence, 630 km south-westward to core GS18 (U in Fig. 1A), does not present any major change at 4.2 cal. ka BP but shows a clear event close to 8.2 cal. ka BP. This event is reflected by a drop in the oak percentages and, afterwards, the end of high *Ephedra* values (Bottema, 1986; Djamali, 2008 p. 61). To the north, the closest Holocene pollen record is the oxbow lake of Solenoye Zaimishche, located 800 km from core GS18 (Bolikhovskaya and Kasimov, 2010) (SZ in Fig. 1A). The vegetation, with more cold-loving trees, is too different from that recorded in core GS18 for direct valid comparisons as, for example, the Early Holocene starts with high values of Pinaceae.

5.3. Dinocyst assemblages and environmental parameters

5.3.1. Modern assemblages for the interpretation of past dinocyst assemblages

Modern assemblages of dinocysts are used to calibrate information derived from past datasets. In this sense, de Vernal et al. (2013) have built a large database of samples taken in the Atlantic region. Statistical analyses revealed that the most important forcing factors are summer and winter temperatures, sea ice cover and winter salinity. Unfortunately, no studies have been made on the modern dinocyst assemblages for the middle CS basin so far. Hence it is impossible to quantify dinocyst changes over time in terms of the aforementioned environmental parameters, and therefore only a qualitative approach is used here. Sea ice cover may have been an issue in the Lateglacial only.

For the qualitative interpretation, one has to rely on only eleven modern spectra published in Leroy et al. (2013b), which focus on the south basin. However, these modern spectra do not include an important low salinity taxon, i.e. *P. psilata* that is abundant in cores GS18 and GS05, but almost absent in the TM record, and so appearing only in the deep sea cores. Moreover, *S. cruciformis*, another low-salinity taxon, is rare in this limited dinocyst dataset and is only abundant in the Anzali Lagoon (Leroy et al., 2011) that receives abundant freshwater from its many rivers flowing from the Elburz Mountains.

In fact, the PCA carried out on the GS18 and CP18 dinocyst records highlights an opposite behaviour of *P. psilata*–*S. cruciformis*

versus *I. caspienense* in its first principal component (Fig. 6). On the basis of what is known so far, this is taken to represent a salinity gradient (Fig. 7). As an alternative, palaeo-temperatures will also be briefly discussed below to explain the changes in dinocyst assemblages.

5.3.2. The Khvalynian highstand (>12.44–11.56 cal. ka BP)

The GS18 dinocyst record shows a great abundance of the aforementioned low-salinity taxa *P. psilata* and of *S. cruciformis*, suggesting a highstand, as it has also been reconstructed during the Late Pleistocene and Early Holocene in the Black Sea (Wall and Dale, 1973; Mudie et al., 2007; Marret et al., 2009; Verleye et al., 2009; Bradley et al., 2012; Shumilovskikh et al., 2013). Compared with the GS05 sequence, the salinity was lower in the middle than in the south basin, showing a gradient similar to the present, but more contrasted although in general with much lower percentages of low salinity dinocysts in the south.

Meltwater from the melting of the Eurasian ice sheet and permafrost may come from two main different origins: i) the north basin from proglacial lakes via the Volga River and ii) through the south basin via the Turgay Pass, Aral Sea and the Uzboy River. During the Lateglacial the middle basin received mostly meltwater from the Volga River, as the main flow of meltwater from the Turgay Pass, the Aral Sea and the Amu Darya occurred much earlier, i.e. 90–80 ka ago, as shown by OSL dating of large ice-dammed lake deposits (Mangerud et al., 2001, 2004).

The difference between basins reconstructed from the dinocyst data is likely to derive from the poor mixing between basins because the Apsheron Sill might have been higher than today, as this is a tectonically active zone (Allen et al., 2002). Based on a study of sediment cores and sedimentation rates, Kuprin et al. (2003) proposed that the two basins were separated until as recently as the middle Holocene. They base their assumption on the higher sedimentation rates in the south and on the differences in salinity in the Khvalynian period (Ferronsky et al., 1999; Kuprin and Pirumova, 2002). The lack of reliable chronology in core GS05 for the Khvalynian does not allow confirmation or rebuttal of this. However, it is clear that the sedimentation rate for the Khvalynian part of core GS18 is very high: c. 120–75 cm/ka, although with decreasing values from the Lateglacial towards the beginning of the Holocene (Fig. 3).

Because *S. belerius* has been observed during the Younger Dryas in core GS18 but earlier in core GS05, it cannot be used as an indicator of the Younger Dryas. In the Black Sea, this taxon appears in periods of transition, such as between low salinities and higher salinities between 7.6 and 7.0 cal. ka BP (Marret et al., 2009; Bradley et al., 2012). The first main change in salinity detected in both cores GS18 and GS05 is after the reconstructed Khvalynian highstand, and is the transition to a lowstand, in which *S. belerius* becomes very sparse.

The Younger Dryas cold/dry event (expressed in the pollen diagram) is clearly not synchronous to the Khvalynian highstand (interpreted from the dinocysts) as seen here and even better in core GS05 (Leroy et al., 2013c).

5.3.3. The Mangyshlak lowstand and the beginning of the Holocene (11.56–10.55 cal. ka BP)

The Mangyshlak lowstand, here a 1000 yr-long period, is represented by higher values of *I. caspienense*, although not as high as in the Neocaspian intermediate period and its P/D ratio does not increase as would be expected. This dinozone is slightly more pronounced in the south basin than in the middle basin, as could also be seen in the salinity gradient reconstructed based on the PCA (Fig. 7 for GS18, and Fig. 7 in Leroy et al., 2013c for GS05). It marginally overlaps with the end of the Younger Dryas in core GS05; but it is clearly after the Younger Dryas in core GS18. It is well marked by a sedimentary hiatus in core TM, which is expected considering that core TM is a coastal core and, thus, sensitive to drops in water level lower than present day.

In the Russian literature, the Mangyshlak period is defined by increasing carbonate contents and higher grain size which is especially well expressed in shelf cores and some deep-sea cores (Mayev, 2010). Both in core GS05 (sharp increase up to 61%) and in core GS18 (up to 37%, Fig. 2), the carbonate content increases notably at the beginning of the Mangyshlak zone defined by dinocysts, while magnetic susceptibility values decrease. However, high carbonate contents do not finish by the end of the Mangyshlak dinozone, so carbonates cannot be used here as an indicator of the lowstand end. The particle size, however, does not significantly change in the Mangyshlak zone.

Although the Mangyshlak lowstand is not formally mentioned by the Russian team in the studies on the two other neighbouring long cores from the deep basins (i.e. cores GS04 and GS19, Kuprin et al., 2003), these authors suggest a lowstand at the beginning of the Late Khvalynian: 642–582 cm in which they also recognise a peak of *Ephedra* (Kuprin and Rybakova, 2003).

The causes of the Mangyshlak lowstand are not clearly deciphered yet. It is suggested here that it is most likely to result from a combination of climate and hydrographic changes. A climatic component is apparent from our data such as the reconstructed warm and dry Early Holocene. The warming is felt in the carbonate content (precipitation in surface layer of the sea) and by a change from mechanical to chemical weathering (Mayev, 2010; Pierret et al., 2012). The dry conditions are inferred by the high incidence of bushes, but not yet of trees, at the beginning of the Holocene (Figs. 4 and 7). It is however clear that this climatic component is not sufficient to explain this lowstand because the lowstand ends much earlier than the shrub phase. Therefore a strong hydrographic factor must also have driven this lowstand, especially to allow reflooding well before the end of the dry period.

During the Mangyshlak lowstand no water was overflowing to the Black Sea, in contrast to the previous and following highstand periods. This lack of overflow must have had a significant impact on the Black Sea. Lowstands are reconstructed in the Black Sea for the Lateglacial Interstadial, with also a much-debated second one after the beginning of the Holocene (Hiscott et al., 2007). During the Mangyshlak, the CS lacked an overflow; hence this would have had an influence only on the second Black Sea lowstand.

5.3.4. Early Holocene highstand (10.55–4.11 cal. ka BP)

After the increased salinity of the Mangyshlak lowstand, a very clear change to **nearly freshwater assemblages** occurs in core GS018. This observation is even more evident in core GS05. In core TM, the first millennia of the Holocene (after the hiatus) also exhibit very low salinities. Hence the three sequences suggest a long highstand period, perhaps even with higher water levels than in the Late Khvalynian.

During this highstand, the salinity is clearly **lower in the south than in the middle** basin, showing a gradient opposite to the present. At this time, the melting of the Eurasian ice sheet was over. Therefore water had to come from elsewhere. Channels of the Uzboy, identified in Turkmenistan, allowed water from the Amu Darya to reach the CS (Leroy et al., 2013a). Boroffka et al. (2006) observed a lack of settlements around the Aral Sea during a large part of this CS highstand suggesting a lowstand in the Aral Sea. This is followed by a period with a return of the water in the Aral Sea (7–5 cal. ka BP), but during which a flow to the Uzboy and settlements along the riverbanks are nevertheless still recognised.

The Russian investigations suggest that in the Holocene the two basins were largely separate and that more freshwater was flowing

in the south basin from the northern slopes of the Elburz Mountains and Amu Darya (and W. Himalayas) carrying eroded material (Ferronsky et al., 1999; Kuprin and Pirumova, 2002). If the **sill** was really sufficiently high to completely separate the two basins, then the difference of salinity could be explained by difference in water level. Although this is a very tectonic area, the initial water level was relatively high, therefore requiring a high altitude of the sill. But it is more likely that the sill may have only enabled a restricted exchange of water, allowing for two different water salinities to develop: that of the middle basin more saline because less meltwater and that of the south basin with more freshwater because of the strong influence of the Uzboy/Amu Darya inflow. To sum up, the differences between the salinities in the CS basins are interpreted to be due to different sources of freshwater (Amu Darya in the south versus Volga in the north) and also to a poor mixing (role of the Apsheron Sill) between the two basins. PC2-d could have been reflecting these changes in river origin: Volga versus Amu Darya (Fig. 7).

Debate exists on the penetration of the **Indian Summer Monsoon** (ISM) north-westward towards the Pamirs and the Alay, which are the sources of the Amu Darya (Hagg et al., 2007). The modern Tajikistan is the wettest of the central Asian republics with mountainous regions (the Pamirs) receiving in some places more than 1500 mm of precipitation per year during western disturbances (Syed et al., 2006) (Fig. 1A). Schiemann et al. (2007) have however found a significant contemporaneous relationship between summer runoff in the Amu Darya and Zeravshan rivers and the intensity of the ISM. They do not explain it by the spill-over of ISM precipitation themselves over the Hindu Kush into the Amu Darya basin; but they consider it to be due to increased ice melting during strong ISM. Hence it is proposed here that the amount of freshwater found in the south basin of the CS is in part driven from the melting of the glaciers on the Pamir-Alay Mountains. The water feeding these glaciers is nowadays largely influenced by westerlies. However, in the Early Holocene, it is likely that the ISM was stronger (Owen, 2009). Oberhänsli et al. (2011) have shown that low water levels in the Aral Sea correspond to less melting in the headwaters of the Syr Darya and Amu Darya (Tien Shan and Pamir). These authors suggested that snow-cover extent and snow depth on the Tibetan Plateau and adjacent Central Asian ranges correlate positively to Monsoon strength.

The exact level of the sea in this period (10.55–4.11 cal. ka BP) is not known, although it is suggested here to be as high as during the Late Khvalynian. If it was **higher than the threshold of 26 m asl** (Svitoch, 2012), then the CS probably overflowed the Manych Sill and reached the Black Sea. In the speleothem record of the Sofular cave in northern Turkey, Badertscher et al. (2011) show indirect evidence of water overflow from the CS into the Black Sea for an earlier period at 16.6–14.6 ka BP (^{230}Th dates). Ryan et al. (2003) mention periods of possible overflows of the CS into the Black Sea but they are all older than the Mangyshlak. So, if the dinocyst record may be interpreted in terms of palaeo-salinities and hence of past sea levels, the present results are unexpected; and further research is necessary to confirm it and to detect if the CS overflowed into the Black Sea after the Mangyshlak lowstand.

In this discussion so far we have interpreted the high percentages of *P. psilata* and *S. cruciformis* as **driven mainly by low salinity**, hence reflecting high sea levels. Nevertheless, it is worth briefly discussing (and eliminating) the interpretation of the high percentages of *P. psilata* and *S. cruciformis* in terms of water temperature. In the case of the Early Holocene highstand, these high percentages would mean cold water as in the Late Khvalynian due to its Lateglacial age. However, this is highly unlikely as: 1) high precipitation of carbonates reflects warmer waters (Pierret et al., 2012), and 2) the waters transported by the Amu Darya and Uzboy River from the Pamir-Alay take a *few months* to reach the CS and have sufficient time to *warm up* and reach local temperature after crossing the Kara Kum and Kyzyl Kum deserts (K. Arpe, pers. comm.). Hereafter, the interpretation of salinity as a more significant driving factor than temperature for these two taxa is more likely and it is considered that the waters of the CS are warmer since the beginning of the Holocene.

Although this highstand was long-lasting, 6.44 ka long in core GS18 and 7.3 ka long in core GS05, it seems to have not been homogenous throughout its entire duration. In fact, in the GS18 sequence, the more important presence of freshwater algae up to 8.19 cal. ka BP (Fig. 4) and the decreasing values of *P. psilata* since 7.30 cal. ka BP (Fig. 5) suggest a partition of the highstand: a first period (zones d-2 and d-3) with fresher waters than the following period (zone d-4). In core GS05 a sudden decrease in *P. psilata* occurs at 8.4 cal. ka BP (Leroy et al., 2013c); while TM presents a hiatus from 7.5 to 3.5 cal. ka BP (Leroy et al., 2013a) due to its coastal location and thus is sensitive to sea level decrease (when in the present day range). In brief, the highest levels were reached in the first part of this high stand, with signs of a slow decrease in it second part.

5.3.5. The main change at c. 4.11 cal. ka BP

The main change in the dinocyst assemblages occurs at c. 4.11 cal. ka BP in core GS18 and at 3.9 cal. ka BP in core CP14 (Leroy et al., 2007). This is interpreted as a drop of sea level. This is also illustrated by a hiatus and a gypsum crystal layer at 3.9 cal. ka BP in core TM (Leroy et al., 2013a).

Given the uncertainty in the chronology of the three sequences, this sharp transition, due to the return of the Amu Darya to the Aral Sea (or a decrease of its flow to the CS), may be linked to an impact of the dry 4.2 cal. ka event (Staubwasser and Weiss, 2006; Schmidt et al., 2011). Indeed a buffering, due to the time needed to large water masses to change, may explain the small delay in reaction. Other lakes in the region present similar major fluctuations linked to aridification. For example, the multiproxy record of Lake Van (eastern Turkey) shows a humid climate that ended drastically at c. 4 cal. ka ago (Wick et al., 2003). The Aral Sea record indicates a one-millennium-long sea level drop from 4 to 3 cal. ka BP (Boroffka et al., 2006).

5.3.6. Intermediate levels of the Neocaspian (4.11–<2.43 cal. ka BP and core CP18)

The dinocyst assemblages resemble modern CS assemblages since 4.11 cal. ka BP. The 2.6 cal. ka BP highstand (Kroonenberg et al., 2007), Medieval lowstand and Little Ice Age highstand (Naderi Beni et al., 2013) occurred during this time period, but are not well recorded here because of the inadequate time resolution and the buffering effect of the deep sea location of the cores.

6. Conclusions

The present palaeoenvironmental reconstruction was performed on a continuous fine-grained sediment sequence taken from a deep part of the Middle basin of the Caspian Sea. It is essential to separate changes in the terrestrial realm as reconstructed from pollen and spores, from those happening in the water body as reconstructed by dinocysts, because they are not synchronous and have different drivers. However, using the dinocysts as a (semi)-quantitative proxy for salinity remains to be verified by surface sediment properly calibrated by physico-chemical water parameters. In the present study, a pioneer attempt has been proposed to interpret the dinocyst assemblages based on what is currently known, although much remaining to be confirmed.

The main **pollen changes** in core GS18 occur at 8.19 cal. ka BP after a long shrub phase, but also at 11.42 and 3.50 cal. ka BP and are linked to the progressive, but delayed, development of the forest. This is similar to shifts reconstructed in core GS05 (south basin), indicating that the landscape around the CS was changing dramatically at these times. The **dinoflagellate assemblages** in the CS were transformed twice: first from a *S. cruciformis–P. psilata* one to a *I. caspienense*-dominated one c. 4 cal. ka ago; and secondly from the latter assemblage to a *L. machaerophorum*-dominated one at c. 2.8 cal. ka BP. The main shift, at c. 4 cal. ka BP, is also evidenced in the two other Holocene sequences of the CS and may be related to a similar major lake level drop in regional lakes: Lake Van and the Aral Sea. Because of the quasi synchronicity with other sites in SW Asia, the CS is therefore part of a much vaster supra-regional climatic change, likely the 4.2 cal. ka BP event. These results are very important because, as shown by climatic modelling, the presence or absence of the CS has a small, but significant, influence on global climate via the summer jet stream speed (Farley Nicholls and Toumi, 2013). Moreover this sequence, as well as that of core GS05, confirms the clear difference and indeed succession between the Younger Dryas period and the very Early Holocene (Mangyshlak) lowstand.

Lake levels reconstructed indirectly from palaeo-salinities indicate fresher waters in the **middle basin than in the south basin** in the Late Pleistocene; but a salinity gradient reverse to the present one in the first part of the Holocene. The CS levels are currently directly correlated with precipitation over the Volga drainage basin, especially summer precipitation. It is even possible to forecast the CS levels 6–12 months in advance based on the precipitation upstream of the Volga delta (Arpe et al., 2014). However, this link was more complicated in the past, with the indirect additional influence of low latitudes sources of water, such as from the western Himalayas (Pamir-Alay). Therefore the combination of the Volga and the Uzboy, i.e. the Western Eurasian westerlies (and indirectly the western Himalayan monsoon), resulted in CS level changes of large amplitude, which at times were even able to reverse the normal salinity gradient across the sea.

Not only during the high levels of the Late Pleistocene, but also during the first part of the Holocene (for a duration of 6000 yr), our data suggest that the CS overflowed into the Black Sea overtopping the Manych Sill. However the overspill was interrupted for **1000 yr** at the very beginning of the Holocene during the Mangyshlak lowstand. The higher salinities and inferred lake level drop at the very beginning of the Holocene were largely due to an aridification of the climate but nevertheless with a clear hydrographic factor with the temporary loss of the connection to the Amu Darya. The Younger Dryas cold/dry event is independent from the Khvalynian highstand and from the Mangyshlak lowstand.

The Caspian Sea levels are clearly not directly related with global sea level changes forced by Milankovitch factors; they are more complex, as in addition to climate, a strong hydrographic driver is involved.

Acknowledgements

This study has been conducted within the European Contract INCO-Copernicus “Understanding the Caspian Sea erratic fluctuations” n° IC15-CT96-0112. This was funded by the Centre National de la Recherche Scientifique within the framework of the INSU-DYTEC (DYnamique de la Terre et du Climat) Program (France). Thanks are due to the French and Russian colleagues, who organised and participated in the coring and hydrological sea expedition of August 1994. P.-J. Giannesini kindly provided the carbonate data and he and E. Moreno are the curators of the cores at the Museum National d'Histoire Naturelle de Paris, France. We are especially grateful to P. Tucholka, F. Guichard and K. Arpe who actively contributed to the scientific part of this project. G. Seret (UCL, Belgium) had the first set of palynological residues of core GS18 made available for counting. LLM was funded by the Brunel IfE MINT scheme. The publication is a contribution to the INQUA QuickLakeH project (No. 1227) and to the European project Marie Curie, CLIMSEAS-PIRSES-GA-2009-247512. M. Turner (Brunel University) has kindly checked the English of the manuscript.

Appendix A. Supplementary data

Supplementary data related to this article can be found at http://dx.doi.org/10.1016/j.quascirev.2014.07.011.

References

Allen, M.B., Jones, S., Ismail-Zadeh, A., Simmons, M., Anderson, L., 2002. Onset of subduction as the cause of rapid Pliocene-Quaternary subsidence in the South Caspian basin. Geology 30 (9), 775–778.

Arpe, K., Leroy, S.A.G., Lahijani, H., Khan, V., 2012. Impact of the European Russia drought in 2010 on the CS level. Hydrol. Earth Syst. Sci. 16, 19–27.

Arpe, K., Leroy, S.A.G., Mikolajewicz, U., 2011. A comparison of climate simulations for the last glacial maximum with three different versions of the ECHAM model and implications for summer-green tree refugia. Clim. Past 7, 91–114.

Arpe, K., Leroy, S.A.G., Wetterhall, F., Khan, V., Hagemann, S., Lahijani, H., 2014. Prediction of the CS Level using ECMWF seasonal forecast and reanalysis. Theor. Appl. Climatol. 117, 41–60. http://dx.doi.org/10.1007/s00704-013-0937-6.

Badertscher, S., Fleitmann, D., Cheng, H., Edwards, R.L., Gökturk, O.M., Zumbuhl, A., Leuenberger, M., Tuysuz, O., 2011. Pleistocene water intrusions from the Mediterranean and CSs into the Black Sea. Nat. Geosci. 4, 236–239.

Bennett, K., 2007. Psimpoll and Pscomb Programs for Plotting and Analysis. Version Psimpoll 4.27. http://chrono.qub.ac.uk/psimpoll/psimpoll.html (Last accessed 12.12.13.).

Bezrodnykh, Yu.P., Romanyuk, B.F., Deliya, S.V., Magomedov, R.D., Sorokin, V.M., Parunin, O.B., Babak, E.V., 2004. Biostratigraphy and structure of the Upper Quaternary deposits and some paleogeographic features of the North Caspian Region. Stratigr. Geol. Correl. 12 (1), 102–111.

Birks, H.J.B., Lotter, A.F., Juggings, S., Smol, J.P. (Eds.), 2012. Tracking Environmental Change Using Lake Sediments, vol. 5. Kluwer Academic Publishers, Dordrecht, The Netherlands.

Blaauw, M., 2010. Methods and code for “classical” age-modelling of radiocarbon sequences. Quat. Geochronol. 5 (5), 512–518.

Bolikhovskaya, N.S., Kasimov, N., 2010. The evolution of climate and landscapes of the Lower Volga region during the Holocene. GES 2–10, 78–97. http://int.rgo.ru/wp-content/uploads/2010/07/GES1-10.pdf (Last accessed 10.12.13.).

Boomer, I., von Grafenstein, U., Guichard, F., Bieda, S., 2005. Modern and Holocene sublittoral ostracod assemblages (Crustacea) from the CS: a unique brackish, deep-water environment. Palaeogeogr. Palaeoclimatol. Palaeoecol. 225, 173–186.

Boroffka, N., Oberhänsli, H., Sorrel, P., Demory, F., Reinhardt, C., Wünnemann, B., Alimov, K., Baratov, S., Rakhimov, K., Saparov, N., Shirinov, T., Krivonogov, S.K., Röhl, U., 2006. Archaeology and climate: settlement and lake-level changes at the Aral Sea. Geoarchaeol. Int. J. 21 (7), 721–734.

Bottema, S., 1986. A Late Quaternary pollen diagram from Lake Urmia (Northwestern Iran). Rev. Palaeobot. Palynol. 47, 241–261.

Bradley, L., Marret, F., Mudie, P., Aksu, A., Hiscott, R., 2012. Constraining Holocene sea-surface conditions in the southwestern Black Sea using dinoflagellate cysts. J. Quat. Sci. 27 (8), 835–843.

Chalié, F., and the Caspian Sea INSU-DYTEC Program Members: Escudié, A.S., Badaut-Trauth, D., Blanc, G., Blanc-Valleron, M.M., Brigault, S., Desprairies, A., Ferronsky, V.I., Giannesini, P.J., Gibert, E., Guichard, F., Jelinowska, A., Massault, M., Mélières, F., Tribovilllard, N., Tucholka, P., Gasse, F., 1997. The glacial-post glacial transition in the southern Caspian Sea. C. R. l'Acad. Sci. Paris, série 2a 324, serie IIa, 309–316.

Chepalyga, A.L., 2007. The late glacial great flood in the Ponto-Caspian basin. In: Yanko-Hombach, V., Gilbert, A.S., Panin, N., Dolukhanov, P. (Eds.), The Black Sea Flood Question: Changes in Coastline, Climate and Human Settlement. Springer, Dordrecht, pp. 119–148.

Connor, S.E., 2006. A Promethean Legacy: Late Quaternary Vegetation History of Southern Georgia, Caucasus (PhD thesis). University of Melbourne, Australia, p. 327.

de Vernal, A., Rochon, A., Fréchette, B., Henry, M., Radi, T., Solignac, S., 2013. Reconstructing past sea ice cover of the Northern Hemisphere from dinocyst assemblages: status of the approach. Quat. Sci. Rev. 79, 122–134.

Djamali, M., 2008. Palaeoenvironmental Changes in Iran during the Last Two Climatic Cycles (Vegetation-climate-anthropisation) (Doctoral thesis). Université Paul Cézanne (Aix – Marseille III), France, p. 194.

Farley Nicholls, J., Toumi, R., 2013. On the lake effects of the Caspian Sea. Q. J. R. Meteorol. Soc. http://dx.doi.org/10.1002/qj.2222.

Ferronsky, V.I., Polyakov, V.A., Kuprin, P.N., Lobov, A.L., 1999. The nature of variations in the level of the Caspian Sea (based on bottom-sediment data). Water Resour. 26 (6), 583–596.
Froehlich, K., Rozanski, K., Povinec, P., Oregioni, B., Gastaud, J., 1999. Isotope studies in the Caspian Sea. Sci. Total Environ. 237/238, 419–427.
Ginzburg, A.I., Kostianoy, A.G., Sheremet, N.A., 2005. Sea surface temperature variability. In: Kostianoy, A., Kosarev, A. (Eds.), The Caspian Sea Environment. Springer, Berlin Heidelberg, pp. 59–81.
Giralt, S., Julià, R., Leroy, S., Gasse, F., 2003. Cyclic water level oscillations of the KaraBogaz Gol – Caspian Sea system. Earth Planet. Sci. Lett. 212 (1–2), 225–239.
Hagg, W., Braun, L.N., Kuhn, M., Nesgaard, T.I., 2007. Modelling of hydrological response to climate change in glacierized Central Asian catchments. J. Hydrol. 332, 40–53.
Hammer, Ø., Harper, D.A.T., Ryan, P.D., 2001. PAST: paleontological statistics software package for education and data analysis. Palaeontol. Electron. 4 (1), 9. http://palaeo-electronica.org/2001_1/past/issue1_01.htm (last accessed 3.04.14.).
Hiscott, R.N., Aksu, A.E., Mudie, P.J., Marret, F., Abrajano, T., Kaminski, M.A., Evans, J., Çakıroglu, A.I., Yasar, D., 2007. A gradual drowning of the southwestern Black Sea shelf: evidence for a progressive rather than abrupt Holocene reconnection with the eastern Mediterranean Sea through the Marmara Sea Gateway. Quat. Int. 167–168, 19–34.
Jackson, J., Priestley, K., Allen, M., Berberian, M., 2002. Active tectonic of the South Caspian Basin. Geophys. J. Int. 148, 214–245.
Jelinowska, A., Tucholka, P., Guichard, F., Lefèvre, I., Badaut-Trauth, D., Chalié, F., Gasse, F., Tribovillard, N., Desprairies, A., 1998. Mineral magnetic study of late Quaternary South Caspian Sea sediments, palaeoenvironmental implications. Geophys. J. Int. 133, 499–509.
Jelinowska, A., Tucholka, P., Badaut-Trauth, D., 1999. Magnetic mineral variations of South Caspian Sea sediments at laminae scale. Phys. Chem. Earth (A) 24, 823–828.
Kazancı, N., Gulbabazadeh, T., Leroy, S., Ileri, O., 2004. Sedimentary and environmental characteristics of the Gilan-Mazenderan plain, northern Iran: influence of long- and short-term Caspian water level fluctuations on geomorphology. J. Mar. Syst. 46 (1–4), 145–168.
Klige, R.K., 1990. Historical changes of the regional and global hydrological cycles. GeoJournal 20.2, 129–136.
Kosarev, A.N., 2005. Physico-geographical conditions of the Caspian Sea. In: Hutzinger, O. (Ed.), The Handbook of Environmental Chemistry, Water Pollution, Part P, vol. 5. Springer, Berlin, pp. 5–31.
Kosarev, A.N., Yablonskaya, E.A., 1994. The Caspian Sea. SPB Academic Publishing, The Hague, p. 176.
Kostianoy, A., Kosarev, A., 2005. The Caspian Sea Environment. Springer, Berlin Heidelberg, p. 271.
Kroonenberg, S.B., Abdurakhmanov, G.M., Badyukova, E.N., van der Borg, K., Kalashnikov, A., Kasimov, N.S., Rychagov, G.I., Svitoch, A.A., Vonhof, H.B., Wesselingh, F.P., 2007. Solar-forced 2600 BP and Little Ice Age highstands of the Caspian Sea. Quat. Int. 173–174, 137–143.
Kuprin, P.N., Ferronsky, V.I., Popovchak, V.P., Shlykov, V.G., Zolotaya, L.A., Kalisheva, M.V., 2003. Bottom sediments of the Caspian Sea as an indicator of changes in its water regime. Water Resour. 30 (2), 136–153.
Kuprin, P.N., Pirumova, L.G., 2002. Synchronous changes in the diatom complexes and hydrological conditions in the Middle and Southern Caspian paleobasins. Water Resour. 29 (6), 605–621.
Kuprin, P.N., Rybakova, N.O., 2003. Analysis of palynological complexes of deep-sea sediments in the Middle and Southern Caspian. Water Resour. 30 (1), 1–9.
Lahijani, H.A.K., Tavakoli, V., Amini, A.H., 2008. South Caspian river mouth configuration under human impact and sea level fluctuations. Environ. Sci. 5 (2), 65–86.
Leroy, S.A.G., 2010. Palaeoenvironmental and palaeoclimatic changes in the Caspian Sea region since the Lateglacial from palynological analyses of marine sediment cores. Geogr. Environ. Sustain. Faculty of Geography of Lomonosov Moscow State University and by the Institute of Geography of RAS 2, 32–41.
Leroy, S.A.G., Arpe, K., 2007. Glacial refugia for summer-green trees in Europe and S-W Asia as proposed by ECHAM3 time-slice atmospheric model simulations. J. Biogeogr. 34, 2115–2128.
Leroy, S.A.G., Kakroodi, A.A., Kroonenberg, S.B., Lahijani, H.A.K., Alimohammadian, H., Nigarov, A., 2013a. Holocene vegetation history and sea level changes in the SE corner of the Caspian Sea: relevance to SW Asia climate. Quat. Sci. Rev. 70, 28–47.
Leroy, S.A.G., Lahijani, H.A.K., Djamali, M., Naqinezhad, A., Moghadam, M.V., Arpe, K., Shah-Hosseini, M., Hosseindoust, M., Miller, Ch.S., Tavakoli, V., Habibi, P., Naderi, M., 2011. Late Little Ice Age palaeoenvironmental records from the Anzali and Amirkola lagoons (south Caspian Sea): vegetation and sea level changes. Palaeogeogr. Palaeoclimatol. Palaeoecol. 302, 415–434.
Leroy, S.A.G., Lahijani, H.A.K., Reyss, J.-L., Chalié, F., Haghani, S., Shah-Hosseini, M., Shahkarami, S., Tudryn, A., Arpe, K., Habibi, P., Nasrollahzadeh, H.S., Makhlough, A., 2013b. A two-step expansion of the dinocyst *Lingulodinium machaerophorum* in the Caspian Sea: the role of changing environment. Quat. Sci. Rev. 77, 31–45.
Leroy, S.A.G., Marret, F., Gibert, E., Chalié, F., Reyss, J.-L., Arpe, K., 2007. River inflow and salinity changes in the Caspian Sea during the last 5500 years. Quat. Sci. Rev. 26, 3359–3383.
Leroy, S.A.G., Marret, F., Giralt, S., Bulatov, S.A., 2006. Natural and anthropogenic rapid changes in the Kara-Bogaz Gol over the last two centuries by palynological analyses. Quat. Int. 150, 52–70.
Leroy, S.A.G., Tudryn, A., Chalié, F., López-Merino, L., Gasse, F., 2013c. From the Allerød to the mid-Holocene: palynological evidence from the south basin of the Caspian Sea. Quat. Sci. Rev. 78, 77–97.
Mangerud, J., Astakhov, V.I., Jacobsson, M., Svendsen, J.I., 2001. Huge Ice-Age lakes in Russia. J. Quat. Sci. 16, 773–777.
Mangerud, M., Jakobsson, M., Alexanderson, H., Astakhov, V., Clarke, G.K.C., Henriksen, M., Hjort, C., Krinner, G., Lunkka, J.-P., Möller, P., Muray, A., Nikolskaya, O., Saarnisto, M., Svendsen, J.I., 2004. Ice-dammed lakes and rerouting of the drainage of northern Eurasia during the Last Glaciation. Quat. Sci. Rev. 23, 1313–1332.
Marret, F., Leroy, S., Chalié, F., Gasse, F., 2004. New organic-walled dinoflagellate cysts from recent sediments of central Asian seas. Rev. Palaeobot. Palynol. 129, 1–20.
Marret, F., Mudie, P., Aksu, A., Hiscott, R.N., 2009. A Holocene dinocyst record of a two-step transformation of the Neoeuxinian brackish water lake into the Black Sea. Quat. Int. 197 (1–2), 72–86.
Mayev, E.G., 2010. Mangyshlak regression of the Caspian Sea: relationship with climate. In: Proceedings of the International Conference—The Caspian Region: Environmental Consequences of the Climate Change. October, 14–16, Moscow, Russia. Faculty of Geography, Moscow, pp. 107–109.
McCarthy, F.M.G., Mudie, P.J., 1998. Oceanic pollen transport and pollen: dinocyst ratios as markers of late Cenozoic sea level change and sediment transport. Palaeogeogr. Palaeoclimatol. Palaeoecol. 138, 187–206.
Mertens, K.N., Ribeiro, S., Bouimetarhan, I., Caner, H., Combourieu-Nebout, N., Dale, B., de Vernal, A., Ellegaard, M., Filipova, M., Godhe, A., Grøsfjeld, K., Holzwarth, U., Kotthoff, U., Leroy, S., Londeix, L., Marret, F., Matsuoka, K., Mudie, P., Naudts, L., Peña-manjarrez, J., Persson, A., Popescu, S., Sangiorgi, F., van derMeer, M., Vink, A., Zonneveld, K., Vercauteren, D., Vlassenbroeck, J., Louwye, S., 2009. Process length variation in cysts of a dinoflagellate, *Lingulodinium machaerophorum*, in surface sediments investigating its potential as salinity proxy. Mar. Micropaleontol. 70, 54–69.
Mudie, P.J., Leroy, S.A.G., Marret, F., Gerasimenko, N., Kholeif, S.E.A., Sapelko, T., Filipova-Marinova, M., 2011. Non-pollen palynomorphs: indicators of salinity and environmental change in the Caspian-Black Sea-Mediterranean corridor. In: Buynevich, I., Yanko-Hombach, V., Gilbert A, .S., Martin, R.E. (Eds.), Geology and Geoarchaeology of the Black Sea Region: Beyond the Flood Hypothesis, Geological Society of America Special Paper 473, pp. 89–115.
Mudie, P.J., Marret, F., Aksu, A.E., Hiscott, R.N., Gillespie, H., 2007. Palynological evidence for climatic change, anthropogenic activity and outflow of Black Sea Water during the late Pleistocene and Holocene: centennial- to decadal-scale records from the Black and Marmara Seas. Quat. Int. 167–168, 73–90.
Naderi Beni, A., Lahijani, H., Mousavi Harami, R., Arpe, K., Leroy, S.A.G., Marriner, N., Berberian, M., Ponel, V.A., Djamali, M., Mahboubi, A., Reimer, P.J., 2013. Caspian sea level changes during the last millennium: historical and geological evidences from the south Caspian Sea. Clim. Past 9, 1645–1665.
Oberhänsli, H., Novotná, K., Píšková, A., Chabrillat, S., Nourgaliev, D.K., Kurbaniyazov, A.K., Grygar, T.M., 2011. Variability in precipitation, temperature and river runoff in W Central Asia during the past ~2000 yrs. Glob. Planet. Change 76, 95–104.
Owen, L.A., 2009. Latest Pleistocene and Holocene glacier fluctuations in the Himalaya and Tibet. Quat. Sci. Rev. 28, 2150–2164.
Pierret, M.C., Chabaux, F., Leroy, S.A.G., Causse, C., 2012. A record of Late Quaternary continental weathering in the sediment of the Caspian Sea: evidence from U-Th, Sr isotopes, trace element and palynological data. Quat. Sci. Rev. 51, 40–55.
Putans, V.A., Merklin, L.R., Levchenko, O.V., 2010. Sediment waves and other forms as evidence of geohazards in Caspian Sea. Int. J. Offshore Polar Eng. 20 (4), 1–4.
Reimer, P.J., Bard, E., Bayliss, A., Beck, J.W., Blackwell, P.G., Bronk Ramsey, C., Buck, C.E., Edwards, R.L., Friedrich, M., Grootes, P.M., Guilderson, T.P., Haflidason, H., Hajdas, I., Hatté, C., Heaton, T.J., Hoffmann, D.L., Hogg, A.G., Hughen, K.A., Kaiser, K.F., Kromer, B., Manning, S.W., Niu, M., Reimer, R.W., Richards, D.A., Scott, E.M., Southon, J.R., Turney, C.S.M., van der Plicht, J., 2013. IntCal13 and Marine13 radiocarbon age calibration curves, 0-50,000 years cal BP. Radiocarbon 55, 1869–1887.
Richards, K., Bolikhovskaya, N.S., Hoogendoorn, R.M., Kroonenberg, S.B., Leroy, S.A.G., Athersuch, J., 2014. Reconstructions of deltaic environments from Holocene palynological records in the Volga delta, northern Caspian Sea. Holocene. http://dx.doi.org/10.1177/0959683614540961 (in press).
Rodionov, S.N., 1994. Global and Regional Climatic Interaction: the Caspian Sea Experience. Kluwer Academic Press, Dordrecht.
Ryan, W.B.F., Major, C.O., Lericolais, G., Goldstein, St. L., 2003. Catastrophic flooding of the Black Sea. Annu. Rev. Earth Planet. Sci. 31, 525–556.
Rychagov, G.I., 1997. Holocene oscillations of the Caspian Sea and forecasts based on palaeogeographical reconstructions. Quat. Int. 41–42, 167–172.
Schiemann, R., Glazirina, M.G., Schär, C., 2007. On the relationship between the Indian summer monsoon and river flow in the Aral Sea basin. Geophys. Res. Lett. 34, L05706.
Schmidt, A., Quigley, M., Fattahi, M., Azizi, G., Maghsoudi, M., Fazeli, H., 2011. Holocene settlement shifts and palaeoenvironments on the Central Iranian Plateau: investigating linked systems. Holocene 21 (4), 583–595.
Shiklomanov, I.A., Georgievsky, V.Y., Kopaliani, Z.D., 1995. Water balance of the Caspian Sea and reasons of water level rise in the Caspian Sea. In: UNESCO (Ed.), UNESCO-IHP-IOC-IAEA Workshop on Sea Level Rise and the Multidisciplinary

Studies of Environmental Processes in the Caspian Sea Region. Intergovernmental Oceanographic Commission, Workshop Report N°108-Supplément, Paris (France), pp. 1–27.
Shumilovskikh, L.S., Marret, F., Fleitmann, D., Arz, H.W., Nowaczyk, N., Behling, H., 2013. Eemian and Holocene sea-surface conditions in the southern Black Sea: organic-walled dinoflagellate cyst record from core 22-GC3. Mar. Micropaleontol. 101, 146–160.
Sorrel, P., Popescu, S.-M., Head, M.J., Suc, J.P., Klotz, S., Oberhänsli, H., 2006. Hydrographic development of the Aral Sea during the last 2000 years based on a quantitative analysis of dinoflagellate cysts. Palaeogeogr. Palaeoclimatol. Palaeoecol. 234 (2–4), 304–327.
Staubwasser, M., Weiss, H., 2006. Holocene climate and cultural evolution in late prehistoric–early historic West Asia – introduction. Quat. Res. 66 (3), 372–387.
Svitoch, A.A., 2012. The Caspian Sea shelf during the Pleistocene regressive epochs. Oceanology 52 (4), 526–539.
Syed, F.S., Giorgi, F., Pal, J.S., King, M.P., 2006. Effect of remote forcings on the winter precipitation of central southwest Asia part 1: observations. Theor. Appl. Clim. 86, 147–160.
Tudryn, A., Giannesini, P.-J., Guichard, F., Badaut-Trauth, D., Tucholka, P., Boomer, I., 2014. The role of iron minerals in laminae formation in Late Pleistocene sediments of the Caspian Sea. Quat. Int. Available online 29 April 2013 (in press) http://dx.doi.org/10.1016/j.quaint.2013.04.024.
Tuzhilkin, V.S., Katunin, D.N., Nalbandov, Y.R., 2005. Natural chemistry of Caspian Sea waters. In: Kostianoy, A., Kosarev, A. (Eds.), The Caspian Sea Environment. Springer, Berlin Heidelberg, pp. 83–108.
Tuzhilkin, V.S., Kozarev, A.N., 2005. Thermohaline structure and general circulation of the Caspian Sea waters. In: Kostianoy, A., Kosarev, A. (Eds.), The Caspian Sea Environment. Springer, Berlin Heidelberg, pp. 33–57.
Verleye, T.J., Mertens, K.N., Louwye, S., Artz, H.W., 2009. Holocene salinity changes in the southwestern Black Sea: a reconstruction based on dinoflagellate cysts. Palynology 33, 77–100.
Wall, D., Dale, B., 1973. Paleosalinity relationships of dinoflagellates in the Late Quaternary of the Black Sea – a summary. Geosci. Man. 7, 95–102.
Walter, H., Breckle, S.-W., 1989. Temperate and Polar Zonobiomes of Northern Eurasia. Springer, Berlin.
Wick, L., Lemke, G., Sturm, M., 2003. Evidence of Lateglacial and Holocene climatic change and human impact in eastern Anatolia: high resolution pollen, charcoal, isotopic and geochemical records from the laminated sediments of Lake Van, Turkey. Holocene 13, 665–675.